Next-generation non-local van der Waals density functional

D. Chakraborty,[1,2] K. Berland,[3] and T. Thonhauser[1,2,*]

[1] *Department of Physics, Wake Forest University, Winston-Salem, NC 27109, USA.*
[2] *Center for Functional Materials, Wake Forest University, Winston-Salem, NC 27109, USA.*
[3] *Faculty of Science and Technology, Norwegian University of Life Sciences, Norway.*

(Dated: April 29, 2020)

The fundamental ideas for a non-local density functional theory—capable of reliably capturing van der Waals interactions—were already conceived in the 1990's. In 2004, a seminal paper introduced the first practical non-local exchange-correlation functional called vdW-DF, which has become widely successful and laid the foundation for much further research. However, since then, the functional form of vdW-DF has remained unchanged. Several successful modifications paired the original functional with different (local) exchange functionals to improve performance and the successor vdW-DF2 also updated one internal parameter. Bringing together different insights from almost two decades of development and testing, we present the next-generation non-local correlation functional called vdW-DF3, in which we change the functional form while staying true to the original design philosophy. Although many popular functionals show good performance around the binding separation of van der Waals complexes, they often result in significant errors at larger separations. With vdW-DF3, we address this problem by taking advantage of a recently uncovered and largely unconstrained degree of freedom within the vdW-DF framework that can be constrained through empirical input, making our functional semi-empirical. For two different parametizations, we benchmark vdW-DF3 against a large set of well-studied test cases and compare our results with the most popular functionals, finding good performance in general for a wide array of systems and a significant improvement in accuracy at larger separations. Finally, we discuss the achievable performance within the current vdW-DF framework, the flexibility in functional design offered by vdW-DF3, as well as possible future directions for non-local van der Waals density functional theory.

I. INTRODUCTION

Systems with van der Waals interactions are ubiquitous in nature and they determine the structure of a vast and diverse array of materials around us, reaching from cement to DNA. These materials are often of scientific and technological importance, such as for gas storage and sequestration [1–3], sensing [4], catalysis [5], organic electronics [6, 7], and molecular crystals in pharmaceutical [8], ferroelectric [9, 10], and photovoltaic applications [11, 12]. It is therefore surprising that capturing these interactions with standard materials modeling techniques such as density functional theory (DFT) is still very challenging. Thus, a major effort has been devoted to the inclusion of van der Waals forces within DFT over the last two decades [13–30]. Within these developments, the non-local vdW-DF family of functionals was a major breakthrough and stands out in that it can be evaluated from knowledge of the density alone [27–31]. It became popular due to its ability to provide accurate results for binding energies and geometries of systems involving widely different chemical compositions, ranging from typical van der Waals complexes to adsorption on metallic surfaces [29, 30, 32]. However, the emphasis in vdW-DF's design has always been on accurately describing systems at typical van der Waals separations, i.e. 3–4 Å. As a result, errors in interaction energies for larger—but yet still relevant—separations often exceed the 100% mark [33–35]. With the more recent shift in research focus to truly extended systems such as layered materials and surface adsorption, this issue becomes highly pertinent.

The vdW-DF framework was published in 2004 [27], with the original functional form referred to here as vdW-DF1. Later improvements [36–41] focused on optimizing the local exchange with which vdW-DF is paired, while the successor vdW-DF2 [42, 43] also updated an internal parameter in the non-local correlation part. All of these improvements provided essential insight that informed the direction of further research and eventually led to our current development. Overall, the vdW-DF family is remarkably successful and widely used; considering the framework itself and all its offsprings [27, 28, 36–41, 43–46], to date it has received more than 11,000 citations.

However, all improvements of vdW-DF thus far have left its fundamental framework unchanged since its inception. Here, we present an updated framework for next-generation van der Waals density functionals. This new framework is entirely built on the original framework [27, 29], which is rigorously derived from a many-body starting point [30, 47–50], and observes all the same constraints. In our new development, we utilize a recently uncovered and largely unconstrained degree of freedom in the underlying vdW-DF plasmon dispersion model [51]. This newly found flexibility allows us to design a new functional form with two new parameterizations that improve the performance at important mid-range and larger separations *without* sacrificing performance at binding separations—overcoming this long-standing issue. We achieve this by constraining this new degree of freedom in the plasmon dispersion model through optimization

* E-mail: thonhauser@wfu.edu

to accurate quantum chemistry results for reference systems. Our new non-local correlation functional form is a logical extension and successor of the original vdW-DF1 [27] and vdW-DF2-type [43] functionals and hence we call it vdW-DF3.

II. THEORY

A. Lessons Learned from Successive Developments of vdW-DF

The original vdW-DF1 of 2004 was of tremendous importance in establishing the ability to describe van der Waals forces at the pure DFT level. It introduced a non-local correlation energy functional of the electron density $n(\mathbf{r})$ taking the form of a six-dimensional integral

$$E_{\rm c}^{\rm nl}[n] = \frac{1}{2}\int d^3\mathbf{r}\int d^3\mathbf{r}'\; n(\mathbf{r})\,\Phi(\mathbf{r},\mathbf{r}')\,n(\mathbf{r}')\;, \qquad (1)$$

where the kernel $\Phi(\mathbf{r},\mathbf{r}')$ connects different regions of space and is derived from the adiabatic connection formula (ACF), see Section II B. This non-local correlation energy functional includes both short- and long-range contributions, but vanishes seamlessly in the homogeneous electron-gas limit. In vdW-DF, the non-local correlation part is therefore paired with that of the local density approximation (LDA), $E_{\rm c}[n] = E_{\rm c}^{\rm LDA}[n] + E_{\rm c}^{\rm nl}[n]$. The exchange part of vdW-DF, on the other hand, is evaluated at the generalized-gradient level (GGA). The GGA exchange can be expressed as a modulation of the LDA exchange as

$$E_{\rm x}^{\rm GGA}[n] = \int d^3\mathbf{r}\; n(\mathbf{r})\,\epsilon_{\rm x}^{\rm hom}\big(n(\mathbf{r})\big)\,F_{\rm x}(s)\;, \qquad (2)$$

where $\epsilon_{\rm x}^{\rm hom}$ is the exchange-per-particle in the homogenous electron gas and the exchange enhancement factor $F_{\rm x}(s)$ is a function of the reduced gradient $s(\mathbf{r}) \propto |\nabla n(\mathbf{r})|/n(\mathbf{r})^{4/3}$. In what follows, we briefly review various vdW-DF developments and draw up a number of lessons learned from them, which—in turn—influenced our functional design.

In vdW-DF1, revPBE exchange [52, 53] was chosen as the GGA exchange. This choice was based on the fact that its rapidly increasing $F_{\rm x}(s)$ in the $s = 0.5-2$ range, as shown in Fig. 1, ensures that nonphysical binding effects in the exchange channel are kept at a minimum [27, 42]. However, the choice of revPBE also leads to a consistent overestimation of binding separations, occasionally causing incorrect bonding predictions [32, 54–56]. After a number of studies had established both the capabilities and shortcomings of vdW-DF1 [29, 57–61], the turn of the previous decade saw a string of important improvements. First, Murray et al. [42] demonstrated that a generally less aggressive but monotonically increasing $F_{\rm x}(s)$ could also be used to avoid the spurious binding in the exchange channel. They did so by reparameterizing the Perdew-Wang functional of 1986 (PW86r) [62] and showed that $F_{\rm x}(s) \propto s^{2/5}$ for large values of s is well suited to reproduce the Hartree-Fock exchange interaction curves beyond binding separations. This insight was used in the design of the successor vdW-DF2 [43], which utilizes PW86R exchange, but also changes an internal parameter from $Z_{ab}^{\rm DF1} = -0.8491$ to $Z_{ab}^{\rm DF2} = -1.887$. This switch effectively reduces the polarizability of a given density region, but more so for highly inhomogenous low-density regions than for high density ones [63]. Through these changes, vdW-DF2 obtains a significantly improved accuracy for molecular dimers; however, for solids, layered, and some adsorption systems, the development did not resolve the overestimation issues of vdW-DF1, which in some cases even worsened [30, 39, 64, 65]. This suprising worsening can be understood largely from the fact that the derivative of $F_{\rm x}(s)$ of PW86r is larger than that of revPBE around $s = 0.5$, see Fig. 1.

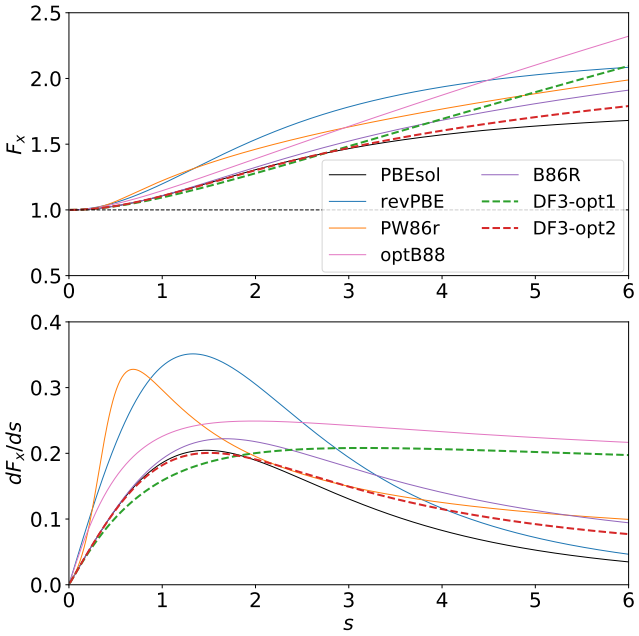

FIG. 1. **(top)** Exchange enhancement factors $F_{\rm x}(s)$ and **(bottom)** their derivatives for selected functionals.

Around the same time, Cooper [36] demonstrated that the systematic overestimation of binding separations could be avoided by using a "soft" exchange functional, i.e. having an exchange enhancement factor $F_{\rm x}(s)$ that increases slowly with s for small values of $s < 1$. To summarize, the following was learned. ■ **Lesson 1:** *The specific shape of $F_{\rm x}(s)$ strongly impacts the bonding in vdW-DF and must be part of any functional design. The small-s limit should be soft, i.e. similar to PBEsol [66], to provide accurate solid lattice constants and $F_{\rm x}(s)$ should increase with s for all values to avoid spurious binding in the exchange channel.* This insight was also used in the optB86b [39] and CX [40] exchange functionals designed for vdW-DF1 and the B86R [67] (see Fig. 1) exchange

functional for vdW-DF2 correlation.

On the other hand, Klimes et al. [37] took a different approach: Instead of updating the non-empirical criteria used in the design of $F_{\rm x}(s)$, they fitted $F_{\rm x}(s)$ directly to the binding energies of the S22 data set of molecular dimers keeping the vdW-DF1 correlation fixed. These variants are therefore labeled as semi-empirical or "reference system optimized". Their approach was surprisingly effective, in the sense that it not only improved binding energies for molecular dimers, as would be expected, but also reduced the overestimation of binding energies and improved performance for several other classes of systems such as adsorption on coinage metals. This is in particular the case for the optB88 [37] functional, which also arrived at a quite soft small-s from, but a very aggressive high-s form. This provides our next lesson. ■ **Lesson 2:** *Within vdW-DF, reference-system optimization to specific benchmark sets has the potential to provide versatile functionals.* A likely reason for this robustness is the soundness of the vdW-DF framework which is based on exact constraints.

As of today, the optB88, optB86b, and CX exchange for vdW-DF1 and B86R for vdW-DF2 are all actively used for broad classes of van der Waals bonded materials and all have quite comparable overall performance, with B86R possibly being slightly better for solids [65], while optB88 is the only one providing satisfactory results for rare gas dimers [68]. ■ **Lesson 3:** *It is not clear whether vdW-DF1 or vdW-DF2 correlation is the best starting point for designing improved functionals, but in any case a suitable exchange partner must be constructed once the correlation functional is updated. In addition, the similar performance of the best vdW-DF1 and vdW-DF2 variants indicate that tuning Z_{ab} is not sufficient to greatly improve performance.* We also note that both B88 and B86b would be suitable starting points for reparameterizations of $F_{\rm x}(s)$. This is less true for CX, as it was designed solely for the vdW-DF1 correlation and is not as widely available in various codes, though this is being remedied [69].

Finally, in our recent work we found that tuning the momentum dependence of the plasmon-pole model within vdW-DF provides an additional degree of freedom that is fully consistent with the original constraint-based design philosophy and that can be used to tailor various aspects of the vdW-DF performance [51]. In particular, we learned two important points. ■ **Lesson 4:** *The plasmon-pole model is the key for improving the ability to simultaneously describe short- and long-range contributions to van der Waals interactions and thus also its ability to describe both small dimers and extended systems accurately. And, the asymptotic behavior of any vdW-DF functional has limited influence on the binding curves over physically relevant distances.*

All these lessons laid the foundation for our design of vdW-DF3.

B. Review of the Original vdW-DF Framework

The kernel $\Phi(\mathbf{r},\mathbf{r}')$ in Eq. (1) can be rigorously derived through a second-order expansion of the ACF. The expansion is in terms of an effective plasmon propagator S, which describes virtual charge-density fluctuations of the electron gas and has poles for real frequencies at the effective plasmon frequency $\omega_{\mathbf{q}}$, where $\mathbf{q}$ is the momentum of the plasmon [27, 30]. Written explicitly including the kernel $\Phi(\mathbf{r},\mathbf{r}')$, Eq. (1) takes the form:

$$E_{\rm c}^{\rm nl}[n] = \int_0^\infty \frac{du}{4\pi} \int \frac{d^3\mathbf{q}}{(2\pi)^3}\frac{d^3\mathbf{q}'}{(2\pi)^3} \times \left[1-(\hat{\mathbf{q}}\cdot\hat{\mathbf{q}}')^2\right] S_{\mathbf{q},\mathbf{q}'}(iu) S_{\mathbf{q}',\mathbf{q}}(iu)\,, \quad (3)$$

where S is given by:

$$S_{\mathbf{q},\mathbf{q}'}(\mathrm{i}u) = \frac{1}{2}\Big[\tilde{S}_{\mathbf{q},\mathbf{q}'}(\mathrm{i}u) + \tilde{S}_{-\mathbf{q}',-\mathbf{q}}(\mathrm{i}u)\Big] \quad (4a)$$

$$\tilde{S}_{\mathbf{q},\mathbf{q}'}(\mathrm{i}u) = \int d^3\mathbf{r}\, \frac{e^{-\mathrm{i}(\mathbf{q}-\mathbf{q}')\cdot\mathbf{r}}\, 4\pi n(\mathbf{r})}{\big(\mathrm{i}u+\omega_{\mathbf{q}}(\mathbf{r})\big)\big((-\mathrm{i}u+\omega_{\mathbf{q}'}(\mathbf{r})\big)} \quad (4b)$$

Here, $u=-\mathrm{i}\,\omega$ is the imaginary frequency and $4\pi n(\mathbf{r})$ is the square of the classical plasmon frequency. Note that there are two symmetric two-point S in Eq. (3), each of which contains one density and one spatial integral (see Eq. (4b)), leading to the two densities and spatial integrals in Eq. (1). This particular form of S is chosen such that it can fulfill four important physical constraints, i.e. time invariance, charge conversation, the f-sum rule, and maintaining self-correlation at large q [27, 30]. These constrains are at the heart of vdW-DF and make it a powerful and transferable tool for capturing van der Waals interactions in vastly different systems.

As the main ingredient in Eq. (4b), the dispersion model for $\omega_{\mathbf{q}}$ comes into focus. The small-q limit of $\omega_{\mathbf{q}}$ has to be a constant (i.e. independent of q). On the other hand, for the choice of S in Eq. (4b), the above constraints are fulfilled if the plasmon dispersion has the large-q limit of $\lim_{q\to\infty}\omega_{\mathbf{q}}(\mathbf{r}) = q^2/2$. For q values in-between, the dispersion is not known. As such vdW-DF uses a switching function h that smoothly switches between the two known limits. In particular, vdW-DF defines for the plasmon dispersion

$$\omega_{\mathbf{q}}(\mathbf{r}) = \frac{q^2}{2}\cdot\frac{1}{h\big(q/q_0(\mathbf{r})\big)}\,, \quad (5)$$

where the switching function h determines the relation between density-density fluctuations and electromagnetic induction at different length scales. To facilitate the numerical evaluation, the vdW-DF framework uses only one length scale $\sim 1/q_0\big(n(\mathbf{r})\big)$ in the switching function, which depends on the density and parameterizes the local response of the electron gas. $q_0(\mathbf{r})$ is determined by the requirement that the first-order expansion of the ACF in S reproduces a general gradient approximation-type local exchange-correlation (XC) functional. This XC functional is referred to as the *internal functional*, $\epsilon_{\rm xc}^{\rm int}$, and

is in general different from the total exchange-correlation functional. The first-order expansion then yields for the internal functional [27]

$$\begin{aligned}\epsilon_{\rm xc}^{\rm int}(\mathbf{r}) &= \pi \int \frac{d^3\mathbf{q}}{(2\pi)^3}\left[\frac{1}{\omega_{\mathbf{q}}(\mathbf{r})} - \frac{2}{q^2}\right] \\ &= 2\pi \int \frac{d^3\mathbf{q}}{(2\pi)^3}\frac{1}{q^2}\left[h\big(q/q_0(\mathbf{r})\big) - 1\right] \\ &= -\frac{1}{\pi}\, q_0(\mathbf{r}) \int_0^\infty dy\,[1-h(y)]\,. \end{aligned} \tag{6}$$

If we set

$$\int_0^\infty dy\,[1-h(y)] = \frac{3}{4}\,, \tag{7}$$

then $q_0(\mathbf{r})$ takes a particularly simple form as a modulation of the Fermi wave vector $k_{\rm F}^3(\mathbf{r}) = 3\pi^2 n(\mathbf{r})$, i.e. $q_0(\mathbf{r}) = -(4\pi/3)\,\epsilon_{\rm xc}^{\rm int}(\mathbf{r}) = \big(\epsilon_{\rm xc}^{\rm int}(\mathbf{r})/\epsilon_{\rm x}^{\rm LDA}(\mathbf{r})\big)\,k_{\rm F}(\mathbf{r})$. For practical purposes, the internal functional is approximated as LDA exchange correlation plus simple quadratic exchange gradient corrections of the form $-Z_{ab}^{\rm DF1(2)} s^2/9$. Both these functionals represent two different directions for design philosophies that are equally valid, but yield varying levels of accuracy for different classes of materials [30].

Obvious constraints on $h(y)$ are Eq. (7) and that $\lim_{y\to\infty} h(y) = 1$ to fulfill the large-q limit of $\omega_{\mathbf{q}}(\mathbf{r})$. A third constraint, i.e. $h(0) = 0$, corresponds to charge conservation of the spherical XC hole model of the internal functional [49]. The original vdW-DF framework chooses a particular simple switching function that fulfills all of those constraints trivially as $h_{\rm orig}(y) = 1 - \exp(-\gamma y^2)$, where $\gamma = 4\pi/9$. However, the three constraints do still leave considerable freedom and more complicated forms of h are conceivable—yet, staying completely within the original framework and thus inheriting its constraint-based transferability.

C. New Development

We have recently demonstrated that the freedom in choosing the h function can be exploited to significantly improve the notoriously bad C_6 coefficients that derive from the vdW-DF framework [51]. From our work it became obvious that this newly found freedom directly translates into a significantly expanded design freedom (Lesson 4). Although our focus in Ref. [51] was on the asymptote, we nonetheless gained some general insight into what aspects of h lead to what outcomes. In this regard, the fixing of the C_6 coefficients was a simpler task, as they are proportional to $\lim_{y\to 0} h(y)/y^2$; the problem of fixing the C_6 coefficients (asymptotic behavior) is thus separable from improving the binding (short-range behavior) and a relatively simple h function is sufficient.

In our new development, we explore a larger space of h functions in order to improve the general accuracy for short, medium, and long separations. This problem is vastly more complicated compared to the C_6 coefficients as it does not separate and competing interests have to be balanced. The accurate description of interactions beyond the binding separation is important for e.g. inter-layer binding and surface adsorption, truly extended systems such as layered systems, or an accurate description of anharmonic vibrational modes or other non-equilibrium processes.

Based on what we learned from our work on the C_6 coefficient, combined with an extensive amount of trial and error, we identified a new switching function which is both smooth and more flexible, in the form of

$$h(y) = 1 - \frac{1}{1 + \gamma y^2 + (\gamma^2 - \beta) y^4 + \alpha y^8}\,. \tag{8}$$

α, β, and γ are adjustable parameters in this model, albeit one of them is constrained by Eq. (7); we describe in Sec. II D how we determine the values of those parameters with the help of an optimization scheme (Lesson 2). This particular form of h has a small-y expansion of the form

$$h(y) = \gamma y^2 - \beta y^4 + (2\beta\gamma - \gamma^3) y^6 + \ldots \tag{9}$$

or equivalently,

$$\begin{aligned}&\omega_{\mathbf{q}}(\mathbf{r}) \sim y^2/h(y) = \\ &= 1/\gamma + \beta y^2/\gamma^2 + (\beta^2/\gamma^3 - 2\beta/\gamma + \gamma) y^4 + \ldots\end{aligned} \tag{10}$$

This allows a clear interpretation of the parameters, as the γ parameter sets the long-range van der Waals interactions, whereas the β parameter is the leading-order term causing damping of van der Waals interactions at shorter ranges. Finally, the αy^8 term ensures that Eq. (7) can be fulfilled without interfering with the series expansions determining the long- and medium-range behavior of the functional. The particular form of h is in part inspired by the so-called vdW-DF-09 from Vydrov and Voorhis [46], which does not fulfill Eq. (7), and was designed just prior to the release of the more well-known VV09 and VV10 [20, 22]. Note that, while Eq. (10) does not contain the exponential term of the original h function, it can be made into a form very similar to $h_{\rm orig}(y)$ in the more relevant $0 < y < 2$ range.

The h function in Eq. (8) provides an independent parameter for the y^2 term in series expansions of $\omega_{\mathbf{q}}(\mathbf{r})$, Eq. (10). This freedom can be beneficial for fine-tuning the strength of the van der Waals interactions in the mid-range, a few Å away from the optimum binding separations. However, when trying to minimize the error in interaction energy of van der Waals complexes from binding distances to mid-range and larger distances, we find the somewhat surprising result that the optimal β is close to 0, so that we actually approximate it with $\beta = 0$. This simplifies Eqs. (8) – (10) and we thus define our h function for vdW-DF3 as

$$h_{\rm DF3}(y) = 1 - \frac{1}{1 + \gamma y^2 + \gamma^2 y^4 + \alpha y^8}\,, \tag{11}$$

which leads to the small-y expansions

$$h_{\mathrm{DF3}}(y) = \gamma y^2 - \gamma^3 y^6 + \ldots \quad (12)$$
$$y^2/h_{\mathrm{DF3}}(y) = 1/\gamma + \gamma y^4 + \ldots \quad (13)$$

The quadratic term in $y^2/h_{\mathrm{DF3}}(y)$ is absent, which correspond to the long-range limit of vdW-DF being well suited to describe the entire long-to-mid range van der Waals interactions; at the same time $\beta = 0$ also allows a sharper damping of van der Waals interactions in the mid-to-short range due to a larger α term, corresponding to a faster increase of h at $y \gtrsim 1$. Note that in this context "long-range" in our design does not correspond to the asymptotic limit, but rather corresponds to separations of about 5 – 6 Å beyond the optimum separation.

Figure 2 compares three different h functions. Although all these switching functions appear very similar when plotted vs. y, a different picture emerges when plotting the physically relevant quantity $y^2/h(y)$, which shows stark difference for $y < 0.8$. As both vdW-DF1 and vdW-DF2 correlation is in use in standard functionals today and their performance is comparable (Lesson 3), for our new functional form we want to explore possibilities for improvements both within the vdW-DF1 *and* vdW-DF2 design philosophies and thus present two different parameterizations, which we call $h_{\mathrm{DF3\text{-}opt1}}$ and $h_{\mathrm{DF3\text{-}opt2}}$. Both functions are nearly constant for $y^2/h_{\mathrm{DF3}}(y)$ within $0 < y < 0.3$, which is related to $\beta = 0$. In contrast, for h_{orig} this function behaves quadratic for small y. All plotted h functions have intercepts at different values $\lim_{y\to 0} y^2/h(y) = 1/\gamma$ because they all have different values for γ. This intercept is directly related to the asymptotic behavior of the functional and different degrees of accuracy for the corresponding C_6 coefficients can thus be expected [51].

Our new switching functions $h_{\mathrm{DF3\text{-}opt1}}$ and $h_{\mathrm{DF3\text{-}opt2}}$ constitute a significant change of the original vdW-DF framework. Any such modifications require careful attention to rebalancing the exchange part in Eq. (2) (Lesson 1). As the exchange largely determines the local screening effects that characterize the chemical binding, we choose to rebalance it through a reparameterization of the free parameters within the enhancement factors $F_{\mathrm{x}}(s)$ of a GGA-based exchange. Since $h_{\mathrm{DF3\text{-}opt1}}$ and $h_{\mathrm{DF3\text{-}opt2}}$ are noticeably different, they both need their own exchange reparameterization. Based on the requirements of the s dependence of F_{x} (Lesson 1), we use

$$F_{\mathrm{x}}^{\mathrm{DF3\text{-}opt1}}(s) = 1 + \frac{\mu s^2}{1 + \mu\, s\, \mathrm{arcsinh}(c\, s)/\kappa} \quad (14)$$
$$F_{\mathrm{x}}^{\mathrm{DF3\text{-}opt2}}(s) = 1 + \frac{\mu s^2}{(1 + \mu s^2/\kappa)^{4/5}}\,, \quad (15)$$

where $c = 2^{4/3}(3\pi^2)^{1/3}$. These exchange functionals are inspired by optB88 [37] and B86R [41], which have previously been paired successfully with vdW-DF1 and vdW-DF2. To describe 'weakly homogeneous' systems, such as solids, layered structures and surfaces, we choose

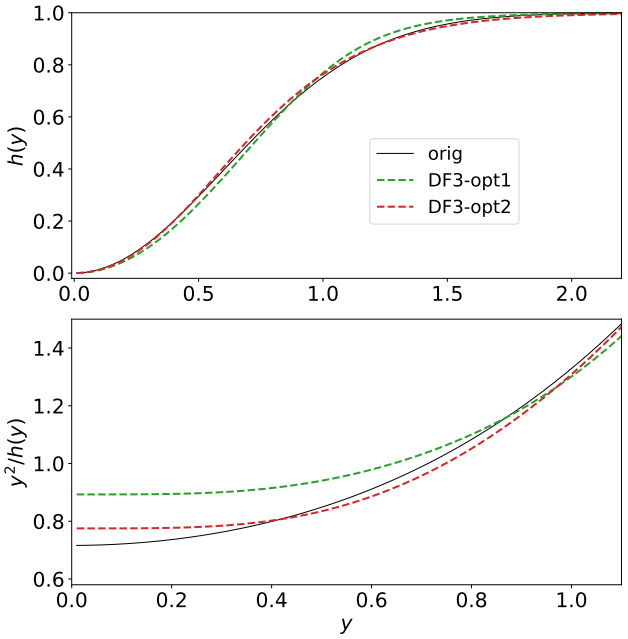

FIG. 2. **(top)** Directly comparing the various h functions shows only minimal changes. **(bottom)** Looking at $y^2/h(y)$, which is proportional to the plasmon dispersion $\omega_{\mathbf{q}}$, is much more revealing. The switching function h_{orig} is taken from Ref. [27]. Note the different scales on the horizontal axes in both panels. The parameters for $h_{\mathrm{DF3\text{-}opt1}}$ and $h_{\mathrm{DF3\text{-}opt2}}$ in Eq. (11) are $(\alpha = 0.94950, \gamma = 1.12)$ and $(\alpha = 0.28248, \gamma = 1.29)$, respectively.

$\mu = \mu_{\mathrm{PBEsol}} = 0.12345$ for both forms (Lesson 1). However, the larger density-gradient region $1 < s < 4$, which directly influences the non-local binding regions, needs to be optimized with respect to our new vdW-DF3 nonlocal functional, which we achieve through including κ in our optimization scheme in Sec. II D. Figure 1 shows the differences in the various enhancement factors and their first derivatives. In both cases, the enhancement factors and their derivatives are reduced at larger gradients $(1 < s < 4)$, indicating that these semi-local exchange functionals become less repulsive at higher density gradients compared to the original functional forms that inspired them, i.e. optB88 and B86R. Finally, we note that both the $F_{\mathrm{x}}(s)$ of DF3-opt2 has a shape that is quite similar to that of B86R and $h(y)$ that is quite similar to that of the original vdW-DF, indicating the suitability of B86R for the vdW-DF2 correlation. DF3-opt1, on the other hand, has no such close similarity with previous functionals.

D. Optimization Scheme

Our original theoretical development leaves three adjustable parameters, i.e. β and γ from the proposed new switching function in Eq. (8)—we constrain α for every pair of β and γ through Eq. (7)—and κ from the en-

hancement factor in Eqs. (14) and (15). Since there are two different enhancement factors with possibly different values for κ, in principle we have to perform two three-dimensional optimizations. We are using a reference-system optimization (Lesson 2), where our parameters are optimized with reference to high-level quantum chemistry (QC) results at the CCSD(T) level of the S22×5 dataset [70]. The quantity to be minimized is the deviation of our calculated interaction energies from the CCDS(T) reference for all 22 systems and all 5 separations. To avoid making the optimization dominated by the large molecular dimers with large binding energies, the target to be minimized should be a relative rather than an absolute energy difference. In particular, we considered the following two measures: mean absolute relative deviation (MARD) and a differently weighted variant which we call weighted mean absolute relative deviation (WMARD), defined as

$$\mathrm{MARD} = \frac{1}{n}\sum_{\mathrm{sep}=1}^{n} \mathrm{MARD}_{\mathrm{sep}} \tag{16}$$

$$\mathrm{WMARD} = \frac{1}{n}\sum_{\mathrm{sep}=1}^{n} \mathrm{WMARD}_{\mathrm{sep}} \tag{17}$$

where

$$\mathrm{MARD}_{\mathrm{sep}} = \frac{1}{m}\sum_{\mathrm{sys}=1}^{m} |E^{\mathrm{DFT}}_{\mathrm{sys,sep}} - E^{\mathrm{QC}}_{\mathrm{sys,sep}}|/E^{\mathrm{QC}}_{\mathrm{sys,sep}} \tag{18}$$

$$\mathrm{WMARD}_{\mathrm{sep}} = \frac{1}{m}\sum_{\mathrm{sys}=1}^{m} |E^{\mathrm{DFT}}_{\mathrm{sys,sep}} - E^{\mathrm{QC}}_{\mathrm{sys,sep}}|/E^{\mathrm{QC}}_{\mathrm{sys,opt}} \tag{19}$$

For the S22×5 set used in our optimization we have $n = 5$ and $m = 22$. Note that MARD puts the deviation in relation to the QC result at that separation and thus treats all separations on the same basis. However, when using MARD we found that the optimization equally weights large percentage deviations at large separations, which, however, may on the absolute scale only be in the sub-meV range—to the detriment of performance around the binding separation. We thus weigh the deviation by the interaction energy at the optimal separation, $E^{\mathrm{QC}}_{\mathrm{sys,opt}}$ (where "opt" is the one separation out of the five for which the interaction energy is largest), and optimize WMARD instead.

The optimization is now performed on a grid for all three parameters, where we use a coarse grid at first and later a finer grid around the minimum. Note that each point in this three-dimensional space requires $22 * 5 + 22 * 2 = 154$ (dimers + monomers) calculations, which quickly becomes cost prohibitive. We thus decouple the exchange degree of freedom from the h-function degrees of freedom and transform the three dimensional optimization into a one-dimensional and two-dimensional optimization. This can be achieved through performing non-selfconsistent calculations and extracting the exchange energy as a function of κ (which is almost entirely independent of β and γ) and the non-local correlation as a function of β and γ (which also to a good approximation can be viewed as independent of κ) [71]. The total energy of any point in the three-dimensional space can then be reconstructed by adding the various contributions on the fly to optimize WMARD. In the end, we verified all our results with fully self-consistent calculations and our numbers reported here in all tables and figures are the results of fully self-consistent calculations. Although this approach constitutes a tremendous reduction in computational effort, we still performed roughly 50,000 non-selfconsistent calculations.

TABLE I. Optimum parameters for vdW-DF3-opt1 and vdW-DF3-opt2. We set β to zero and constrained α through Eq. (7), leaving only γ and κ as adjustable parameters.

functional	h function	α	γ	exchange	κ
DF3-opt1	$h_{\mathrm{DF3\text{-}opt1}}$	0.94950	1.12	$F_{\mathrm{x}}^{\mathrm{DF3\text{-}opt1}}$	1.10
DF3-opt2	$h_{\mathrm{DF3\text{-}opt2}}$	0.28248	1.29	$F_{\mathrm{x}}^{\mathrm{DF3\text{-}opt2}}$	0.58

As mentioned in the previous section, we found optimized β values that are a small positive number and zero, for DF3-opt1 and DF3-opt2, respectively, so we chose to set $\beta = 0$ and thus reduce the amount of parameters in our functionals down to two. Our optimized values for α, γ, and κ are collected in Table I. It is conceivable that the global WMARD minimum, in particular for DF3-opt2, might occur for negative β, but this breaks formal constraints of the vdW-DF construction. Even though β came out to be zero, we chose to present our formalism including β as this provides a rich field of study and a focus on other physical or chemical quantities may well benefit from this degree of freedom, such as reaction chemistry, transition-state searches, or harmonic/unharmonic vibrational excited states and their associated heat transfer.

III. COMPUTATIONAL DETAILS

All our calculations were performed with the QUANTUM ESPRESSO (QE) package [72], where we modified the kernel generation routines to implement our new functionals vdW-DF3-opt1 and vdW-DF3-opt2, and these functionals are now available in the latest official version of QE. We used PBE GBRV ultrasoft pseudopotentials due to their excellent transferability [73]. The wave-function and density cutoffs were set to ∼680 eV (50 Ryd) and ∼8200 eV (600 Ryd), respectively. Self-consistent calculations were performed with an energy convergence criterion of $\sim 1.36\times10^{-7}$ eV (1×10^{-8} Ryd) and, where applicable, a force convergence criterion of $\sim 2.6\times10^{-5}$ eV/Å (1×10^{-6} Ryd/Bohr) was used for structure relaxations. For all calculations including metals/semiconductors a Gaussian smearing with a spread of ∼100 meV (7.35 mRyd) was used. Benchmarking of our new functionals has been done on the molecular dimer datasets S22×5 and S66×8, a set of solids, layered

structures, molecular crystals, and benzene adsorption on Cu/Ag/Au surfaces. We compare the performance of our new functionals with other, well-used dispersion-corrected exchange-correlation functionals such as vdW-DF (vdW-DF1) [27], vdW-DF1-optB88 [37], vdW-DF1-cx [32, 40], vdW-DF2 [43], vdW-DF2-B86R [41], rVV10 [74], and SCAN+rVV10 [75] and we use the following corresponding short names in all tables and figures: DF1, DF1-optB88, DF1-cx, DF2, DF2-B86R, VV, and SCAN+VV, respectively. For the molecular dimers, we calculated all SCAN+VV values; for solids, layered structures, and adsorption on coinage metals we took readily available values from the literature, but for our molecular crystals we found no published SCAN+VV data.

For calculations on the dimer sets, spurious interactions due to the period boundary conditions in QE were minimized by padding dimers and monomers with at least 15 Å of vacuum. A list of 22 metals, semiconductors, and ionic salts were also used as in Ref. [39], except Li. A $15 \times 15 \times 15$ k-point mesh was used for these periodic solids. To calculate their lattice constants and cohesive energies, a Birch-Murnaghan equation-of-state was used and the individual atom energies were calculated in a box surrounded by at least 15 Å of vacuum. Results for cohesive energies and lattice constants are in addition compared to PBE [76] and PBEsol [66]. The reference data on zero-point corrected experimental lattice constants and atomization energies are taken from Ref. [39] and references therein. Several layered structures were also considered. Experimental structures were retrieved from the Inorganic Crystal Structure Database (ICSD). Following the procedure in Refs. [75, 77, 78], these layered structures were relaxed along the inter-layer axis (c-axis) with $12\times12\times6$ k-points, keeping the a-lattice constant at its experimental value. Inter-layer binding energies have been calculated using single layers with fixed a-lattice constant and with at least 12 Å vacuum along the c-axis, using a $12 \times 12 \times 1$ k-mesh. The corresponding reference data is taken from RPA calculations in Ref. [78] and references therein. The molecular crystals benzene, napthalene, anthracene, and tetracene were also studied. Here, calculations were performed starting from experimental structures [12] followed by an optimization of all structural degrees of freedom. Finally, benzene adsorption on the (111) surface of the coinage metals Cu, Ag, and Au have also been used as a benchmark, using the reference data in Refs. [75, 79–82]. Six layers were used to form the metallic slab [79], keeping the three bottom layers fixed and using a 9 Å vacuum. Calculations were performed with a $4 \times 4 \times 1$ k-mesh.

IV. RESULTS

To investigate the performance of vdW-DF3-opt1 and vdW-DF3-opt2, we benchmark those functionals on an extensive list of systems reaching from molecular dimers to periodic systems including solids, layered systems, molecular crystals, and surface adsorption on coinage metals. We compare our results with the most popular functionals, finding good performance in general for a wide array of systems and a significant improvement in accuracy at larger separations.

A. Molecular Dimers

The two adjustable parameters of our functionals (see Table I) have been fitted to minimize the WMARD of the S22×5 dataset [70], as described in Sec. II D. A comparison for this dataset is thus biased by construction, and we will not go into extensive details here. Appendix A holds a statistical summary and detailed results for each dimer are provided in the Supplemental Material [83]. Overall, both our new functionals have a WMARD of less than 4% and perform best in our comparison group. The performance is particularly good for dispersion-dominated complexes. Even though we optimized WMARD, MARD also shows significant improvements.

The more diverse and larger S66×8 set of molecular dimers is our first proper benchmark [84]. Similar to S22×5, this set is comprised of 23 hydrogen bonded complexes, 23 dispersion-dominated complexes, and 20 complexes with various other kinds of interactions. Interaction energies at the CCSD(T) level are reported for eight different separations—two at separations below the optimal binding distance, one at the optimal binding distance, and five separations that are larger, up to twice the optimal binding separation. The WMARD defined in Eq. (17) for the S66×8 set is given in the upper right panel of Fig. 3; a summary of statistical information can be found in Appendix A and detailed results for each dimer are provided in the Supplemental Material [83]. As S66×8 is quite similar to the S22×5 set, our two functionals also here perform best with a WMARD of 4.7% and 4.9%, although it has gone up by approximately one percentile. For hydrogen-bonded complexes, DF3-opt1 has a WMARD of 5.8% which is larger than the others for all but vdW-DF1. However, for dispersion dominated complexes (4.7%) and the remaining complexes (3.5%), DF3-opt1 performs better than all other tested functionals. DF3-opt2 has slightly higher WMARD for dispersion-dominated system (6.2%), but is also very accurate (3.7%) for the rest of the complexes.

A more detailed picture of the performance for the S66×8 emerges in Fig. 3, which provides $\mathrm{WMARD}_{\mathrm{sep}}$ from Eq. (19) , summed over all three subgroups as well as for all 66 complexes. The plots reveal that both DF3-opt1 and DF3-opt2 accurately describe interaction energies at equilibrium separation and beyond for each interaction type. In particular, we consider the "dispersion-dominated" panel amongst the most pertinent results of our study. It shows that DF3-opt1, and to a somewhat lesser extent DF3-opt2, exhibits very good performance for dispersion-bound systems beyond equilibrium separations—whereas several popular functionals

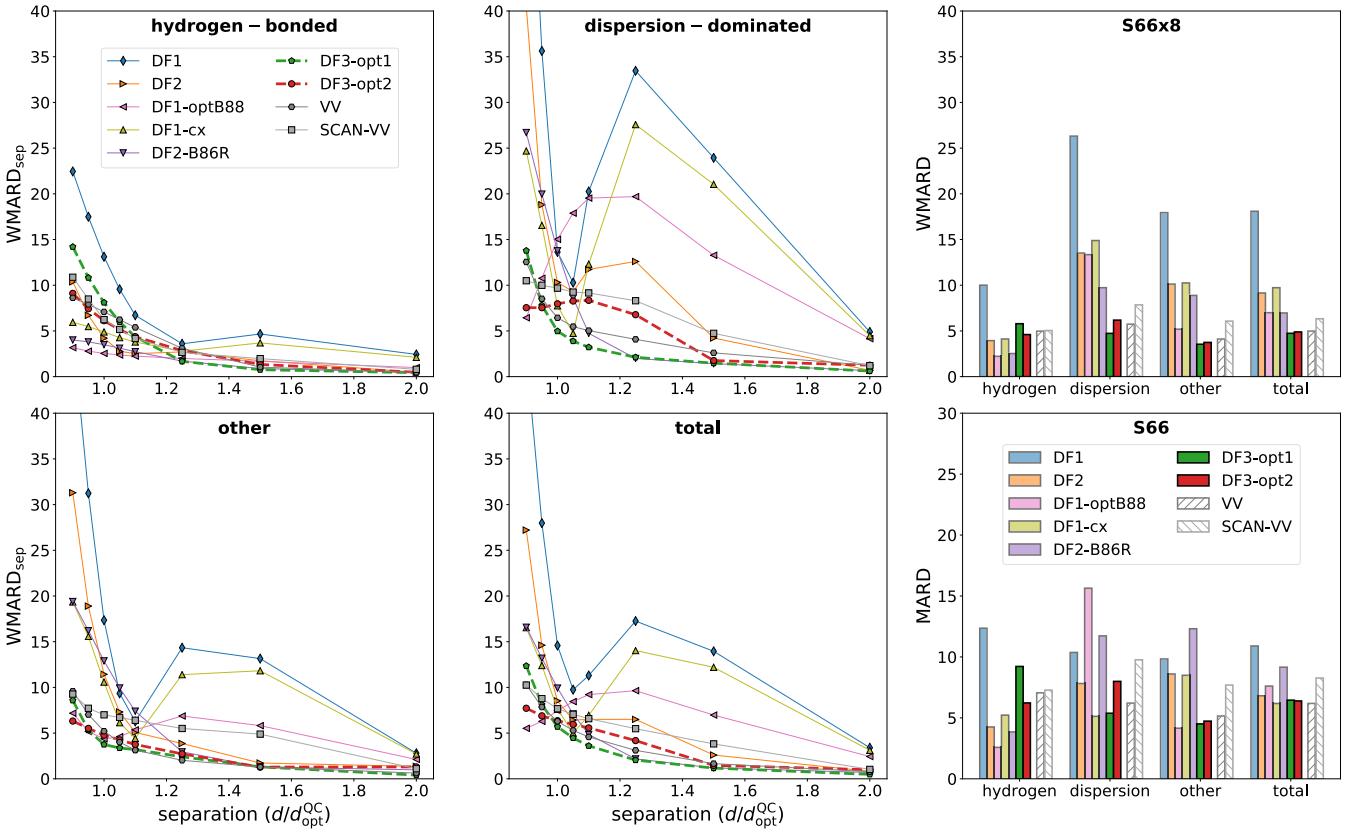

FIG. 3. Statistical analysis for the S66×8 and S66 datasets in reference to QC data at the CCSD(T) level. The four left figures show $\mathrm{WMARD}_{\mathrm{sep}}$ from Eq. (19), summed over different S66×8 subgroups. Separation is given in units of the optimal QC separation $d_{\mathrm{opt}}^{\mathrm{QC}}$. The top right panel shows WMARD from Eq. (17). The bottom right plot shows MARD for the optimal binding energy of the S66 dataset. We compare our results also to VV and SCAN+VV, but we separate them as they are fundamentally different approaches and should not be understood as improvements within the vdW-DF family.

give quite large errors in this regime—and thus confirms that we have achieved our goal of overcoming this long-standing problem. We point out that DF3-opt1 is not the best choice for hydrogen-bonded systems at short separations. DF3-opt2 shows an accuracy quite similar to DF3-opt1, but with somewhat better performance for hydrogen-bonded systems and short separations, at the cost of lower accuracy for dispersion-dominated systems. The reason for the reduced accuracy for hydrogen-bonded systems, in particular for DF3-opt1, may be traced to the smaller $dF_{\mathrm{x}}(s)/ds$ at around $s \approx 0.5-2$ compared to e.g. B86R [40]. Section V provides further discussion on the inherit trade-offs in vdW-DF design.

In addition, we also provide data for the S66 data set [84]—it contains the same molecular dimers as the S66×8 set but uses the optimal binding separation rather than looking at eight explicit separations. Thus, in our comparison, we also fully optimize the binding separation with the various functionals. The MARD of the resulting optimized binding energies is given in the bottom right panel of Fig. 3 and statistical data for the deviations in optimal binding separation and binding energy are analyzed in the left column of Fig. 4 in the form of violin plots and box plots; additional data is available in the Supplemental Material [83]. Again, we find that DF3-opt1 and DF3-opt2 perform very well. In particular, the violin plots reveal that our new functionals provide rather compact results with less spread in comparison to other functionals.

B. Solids

Within DF3-opt1 and DF3-opt2 the non-local correlation is purposefully combined with an exchange energy that has a smaller, PBEsol-like enhancement factor for small s, i.e. $F_{\mathrm{x}}^{\mathrm{DF3\text{-}opt}}(s) = 1 + \mu_{\mathrm{PBEsol}} s^2 + \ldots$. This significantly improves lattice constants as well as atomization energies of solids. In Fig. 4 we collect statistical information in the form of violin plots combined with box plots for a set of 22 standard solids [87] and provide deviations for lattice constants and atomization energies. As reference we use results from zero-point corrected experiments [86]. Here, we also compare with the PBE and

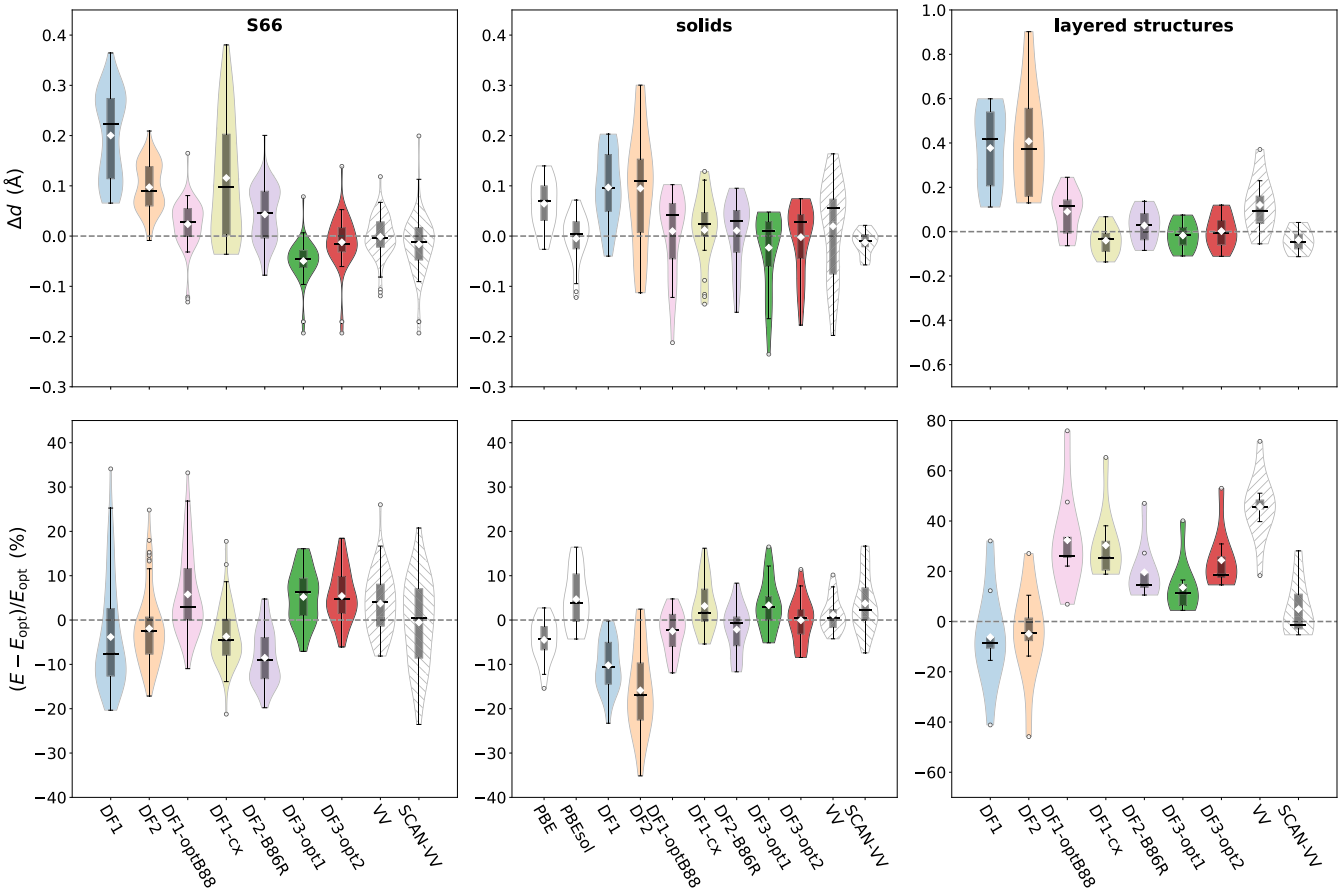

FIG. 4. Violin plots overlaid on box plots of the deviations from reference data for the different functionals. Violin plots represent the data distribution and are based on a Gaussian kernel density estimation using the Scotts rule [85] as implemented in MATPLOTLIB. In the box plot, the boxes hold 50% of the data, with equal number of data points above and below the median deviation (full black line). Whiskers indicate the range of data falling within 1.5×box-length beyond the upper and lower limits of the box. Outliers beyond this range are indicated with circular makers. Diamonds mark the mean deviation. **(left)** Set of 66 molecular dimers: reference data taken from CCSD(T) [84] calculations in form of d (dimer separation) and $E_{\rm opt}$ (binding energy). **(middle)** Set of 22 solids: reference data taken from zero-point corrected experiments [86]; d refers to lattice constant and $E_{\rm opt}$ to atomization energy. **(right)** Set of 9 layered structures: reference data taken from RPA calculations [77, 78]; d refers to layer separation and $E_{\rm opt}$ to layer binding energy. SCAN+VV data for solids and layered structures taken from Ref. [75].

PBEsol functionals often used for solids. Further numerical data is provided in Appendix A. Clearly, PBEsol and SCAN+VV provide an excellent description of lattice constants. However, DF3-opt1 and DF3-opt2, together with other recent functionals also show good performance. In terms of atomization energies, we find several functionals that perform well and even better than PBE, including our new functionals. In particular, DF3-opt2 has a mean and median deviation of essentially zero. Within the vdW-DF family of functionals, DF3-opt1 and DFT-opt2 retain this significant advancement in vdW-DF design, as the original functionals DF1 and DF2 both perform poorly for solids.

C. Layered Structures

We also benchmark our functionals for a set of 9 layered structures against RPA reference calculations [77, 78] and results are given in the right column of Fig. 4; details are provided in Appendix A, also see Ref. [65]. The PBEsol-like enhancement factor for DF3-opt1 and DF3-opt2 that resulted in good lattice constants for solids has an even more prominent effect for layered structures. While the original DF1 and DF2 significantly overestimate the layer separation, much improvement can be seen for all other vdW-DF functionals. In particular, DF3-opt2 has a mean deviation of zero and a compact spread, closely followed by DF3-opt1. Improvements for the layer binding energy are mostly observed in smaller spreads for newer vdW-DF functionals. While SCAN+VV is remarkably good here, DF3-opt1 performs

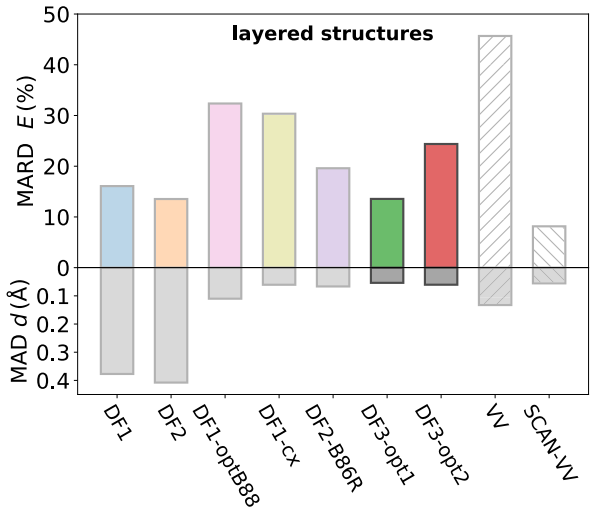

FIG. 5. MARD of layer binding energy and MAD of layer separation for a set of layered structures. SCAN+VV data taken from Ref. [75].

best out of all vdW-DF functionals. The progress made by our two functionals within the vdW-DF family can better be seen in Fig. 5, where we show the MARD of layer binding energy and MAD of layer separation. The original DF1 and DF2 functionals had a reasonable MARD for the energy, but their MAD in layer separation rendered them inapplicable for layered structures. Further developments like DF1-optB88, DF1-cx, and DF2-B86R corrected that behavior, but to the detriment of MARD in energy. DF3-opt1 now noticeably reduces the MARD in energy again (and also the spread, see Fig. 4) while having the lowest MAD in layer separation of any tested functional.

D. Molecular Crystals

An important benchmark for all van der Waals functionals are molecular crystals [12, 30, 65, 88–92]. We have calculated the optimized volume per monomer and cohesive energy per monomer of molecular crystals build from benzene, naphthalene, anthracene, and tetracene. Results are depicted in Fig. 6; a summary of statistical data is available in Appendix A. Looking at the volume, we see that the original DF1 and DF2 show an overestimation, that has been corrected by DF1-optB88 and DF2-B86R. Our new functionals show consistent and noticeable underestimation of the volume. On the other hand, all functionals overestimate the energy, often by significant margins, and DF2-B86R performs best here, followed by DF1-optB88. Similar to the case for hydrogen-bonded systems at short separations in Fig. 3, the mediocre performance of our new functionals may be linked to the shape of $dF_{\rm x}(s)/ds$ around $s \approx 1$ and is the result of a conscious trade-off we made, see the discussion in Section V.

E. Benzene Adsorption on Cu/Ag/Au (111)

Finally, we benchmark our new functionals also against molecular adsorption on coinage metals. In particular, we study the adsorption of benzene on the (111) surface of Cu, Ag, and Au. A summary of statistical data is available in Appendix A. In Fig. 7 we show the benzene adsorption distance from the surface and its adsorption energy. This kind of system is challenging [32] and the original DF1 and DF2 functionals significantly overestimate the binding separations, resulting in dramatic consequences for surface corrugation [93]. This figure also shows nicely the progress that has been made within the vdW-DF family, with DF3-opt1 providing almost perfect distances and very good energies, closely followed by DF3-opt2. This good performance has its roots in the excellence performance for dispersion-dominated systems in Fig. 3 for larger-than-binding separations as the adsorbed molecule interacts with the surface significantly beyond its footprint. This aspect is also intimately linked to—and paralleled by—our improved performance for layered systems.

V. BALANCING COMPETING INTERESTS — WHAT CAN BE EXPECTED FROM THE VDW-DF FRAMEWORK?

The results in the previous sections showed that our new functionals vdW-DF3-opt1 and vdW-DF3-opt2 perform very well. The main advancement is the greatly increased performance for dispersion-dominated molecular dimers, especially at larger-than-binding separations, see Fig. 3. Although we also see improved and generally good performance for many other systems, we would like to point out that performance is only average for e.g. hydrogen-bonded systems at their equilibrium separation. This modest performance might also be related to structural aspects of molecular crystals.

We have noticed this trend early on and investigated measures to also improve performance for hydrogen-bonded systems at the equilibrium separation. These systems are very much controlled by the choice of exchange and we have investigated further parameterized versions of Eq. (14), where changing c in conjunction with κ would, in fact, lead exactly to the desired improvement and we see better performance for hydrogen-bonded dimers and molecular crystals. However, through this higher dimensional parameter search (and other avenues we have investigated) we learned an important lesson: With our new development, the overall vdW-DF framework is coming to its performance limits. Although possible new h-functions provide a rich degree of freedom that allows for improvements of many aspects of particular systems, we now see that further improvements are only possible to the detriment of other areas. In our case, improving the hydrogen-bonded systems at binding separation would lead to a decrease in accuracy for dispersion

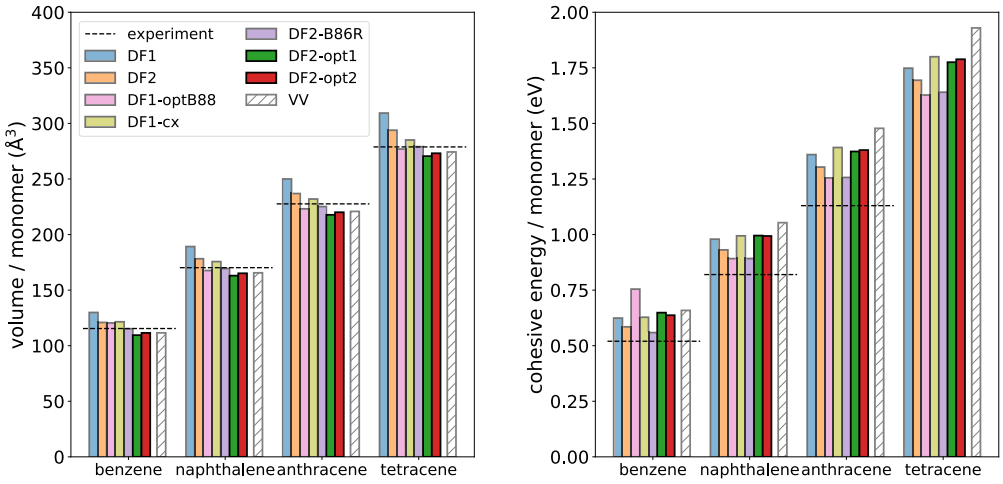

FIG. 6. Optimized volume/monomer (Å^3) and cohesive energy/monomer (eV) for molecular crystals of benzene, napthalene, anthracene, and tetracene. Experimental values are taken from Ref. [12], no experimental value is available for the cohesive energy of tetracene.

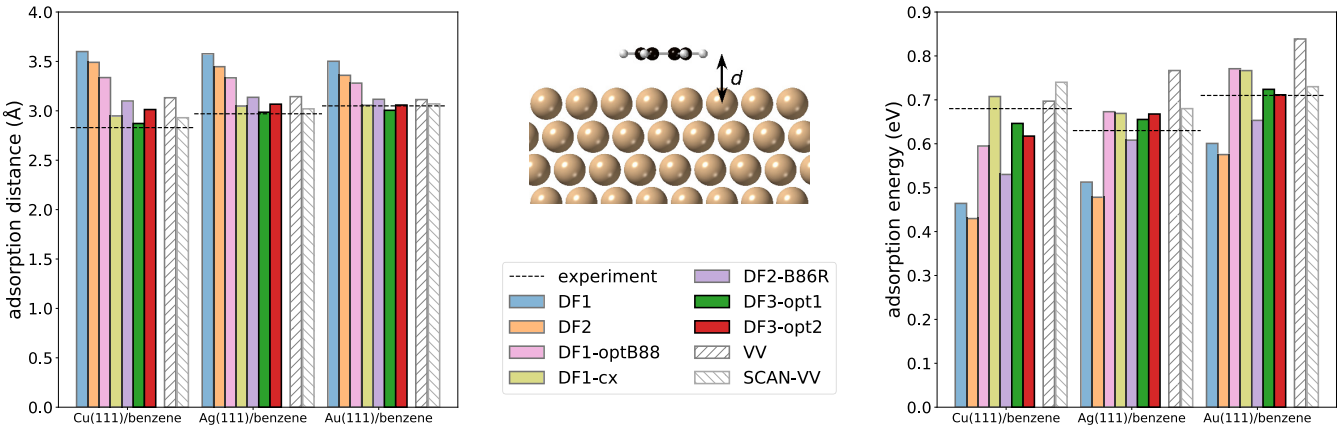

FIG. 7. **(left)** Adsorption distance (Å) and **(right)** adsorption energy (eV) for benzene on Cu, Ag, and Au. Experimental reference values are taken from Ref. [82]. The inset shows the adsorption geometry.

bound dimers, layered systems, and surface adsorption.

We show in Fig. 8 how the balancing of competing interests plays out for the case of hydrogen-bonded molecular dimers vs. dispersion-dominated molecular dimers in Fig. 3. In particular, we study the split-up of the total energy into its non-local contribution E_c^{nl} and the rest E_0, i.e. $E_{tot} = E_c^{nl} + E_0$. Figure 8 shows this split-up as a function of our parameters γ and κ. Our choice for DF3-opt1 was $\kappa = 1.1$ and $\gamma = 1.12$, leading to very good performance for dispersion-dominated systems and less good performance for hydrogen-bonded systems. However, we see that a choice of $\kappa = 1.7$ and $\gamma = 1.4$ would have reversed those roles. As such, even with the same overall optimization scheme leading to the same WMARD minimum, choices have to be made as to what systems are being favored. Our choice fell on dispersion-bonded systems because that was the original target of the vdW-DF development and because of their impact on a large class of relevant problems in surface adsorption and layered structures. On a mechanical level, this was achieved through optimization of the WMARD of the S22×5 set as described in Sec. II D, because the dispersion part is far more sensitive to the parameter choice for the dispersion bonded systems, as can be seen in Fig. 8. The hydrogen-bonded part of WMARD is also significantly smaller in magnitude compared to the dispersion-dominated part.

Through the various improvements of the vdW-DF framework over the years we have reached a point where the performance of the original vdW-DF framework has been pushed to its limit and the fundamental design choices are now becoming the bottleneck. We see two exciting ways forward: (i) New functionals within the vdW-DF family are developed for specific applications, rebalancing our choice. Such functionals would be somewhat limited in scope, but can show very good accuracy for the situation they have been designed. Appli-

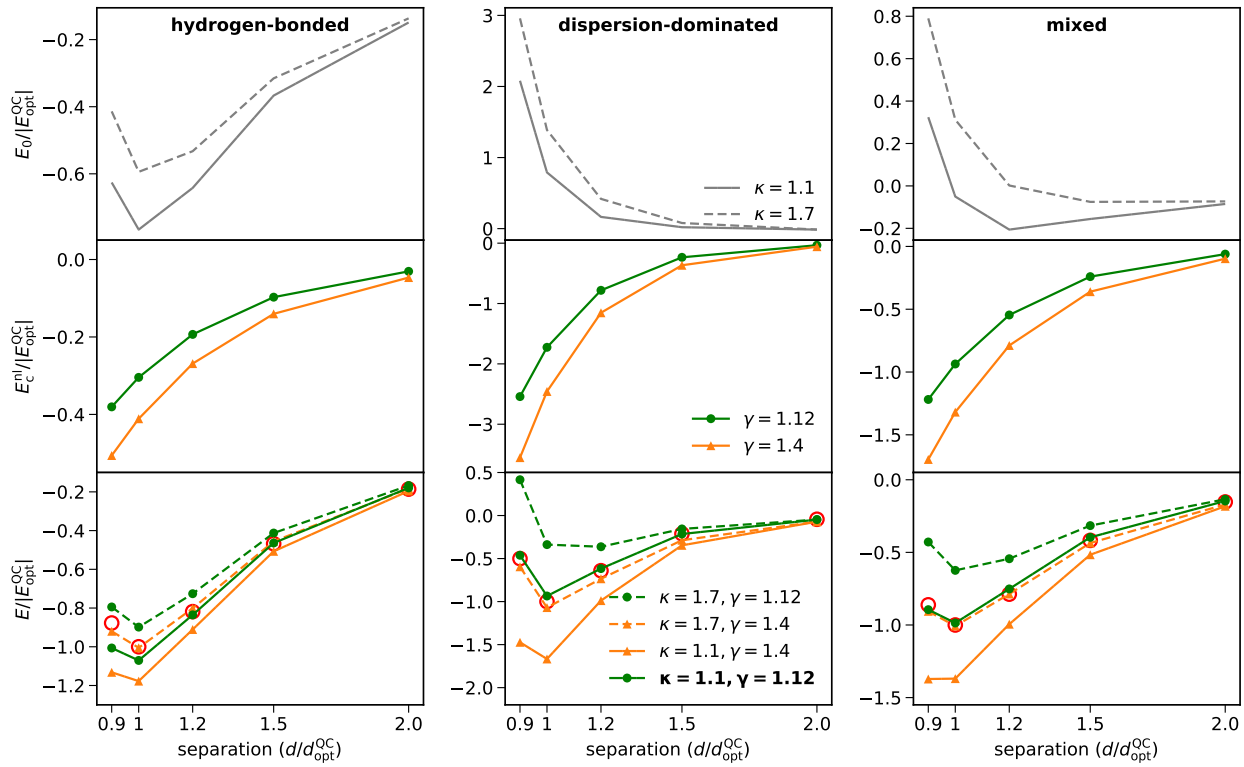

FIG. 8. Split-up of the total energy into its non-local contribution and the rest, i.e. $E_{tot} = E_c^{nl} + E_0$ for hydrogen-bonded, diserpersion-dominated, and mixed dimers of the S22×5 dataset. All energies are reported relative to the QC energy at the optimal separation E_{opt}^{QC} and have been averaged over all dimers in that set. QC reference data is shown by red circles. Lines in the bottom panel "inherit" line style from the top panel and line color from the middle panel. The parameters for DF3-opt1 are $\kappa = 1.1$ and $\gamma = 1.12$.

cations of particular interest may be adsorption systems, molecular crystals, or transition-state chemistry. (ii) Alternatively, it is possible to fundamentally change the vdW-DF framework and deviate from its original design philosophy. We see this as the only option to achieve high accuracy for all systems at the same time and thus truly generate a general-purpose functional. So, where would one even start thinking about such a fundamental change? Below Eq. (5) we point out that vdW-DF uses only a single length-scale to parameterize its plasmon-dispersion model. Already in the 2004 paper we see that this is an approximation made for convenience [27], and the introduction of a second length scale would be beneficial. It is, in fact, surprising that the vdW-DF framework captures such a diverse group of vastly different types of materials so reasonably well. Another possible direction could be to update the rather simple vdW-DF plasmon-dispersion model altogether, maybe along the lines of the VV functionals, from which much can be learned. Finally, it is conceivable that a focus on different physical constraints leads to a more accurate form for S in Eq. (4a) or maybe S could be approximated through better models for the response function. However, common to several of these directions would be that they fundamentally change the vdW-DF framework and design philosophy to such a point that they present completely new directions and thus would likely no longer carry the original vdW-DF name.

VI. CONCLUSIONS

We have presented the next-generation non-local van der Waals density functional vdW-DF3. It is entirely built within the design guidelines of the original vdW-DF, but takes advantage of a newly discovered degree of freedom within the framework to significantly improve performance, in particular for beyond-binding separations. At the same time, we show that—by observing the vdW-DF constraints and building on lessons learned in successive developments—vdW-DF3 can retain the same wide transferability as earlier variants. This finding is based on benchmarking on a wide array of systems, in which we also compare with earlier van der Waals functionals, allowing us to document successive improvements. While we find generally good performance of vdW-DF3 for many systems, the most striking improvement is found for dispersion-dominated systems beyond binding separation. Our analysis also indicates that, with recent developments in general and vdW-DF3 in partic-

ular, the vdW-DF framework is operating close to its limits in terms of overall accuracy. This is also evident through the similarity of the DF3-opt2 parametrization of vdW-DF3 and the DF2-B86R functional. However, as the vdW-DF3 design is more flexible than its predecessors, it opens the door for functionals tailored to more specific classes of systems, which will likely cause some worsening in other areas. Finally, we provide an outlook for research directions that could overcome the fundamental bottlenecks of the vdW-DF framework and lead to further improvements for even broader classes of systems.

ACKNOWLEDGEMENT

This work was supported by the U.S. National Science Foundation Grant No. DMR–1712425. We also thank Tonatiuh Rangel for providing initial molecular crystal structures. Parts of the computations were performed with resources provided by UNINETT Sigma2, the National Infrastructure for High Performance Computing in Norway.

Appendix A: Statistical Data

TABLE II. Comparison of mean deviation (MD), mean absolute deviation (MAD), mean absolute relative deviation (MARD) from Eq. (16) and weighted mean absolute relative deviation (WMARD) from Eq. (17) for the interaction energies of the S22×5 set of molecular dimers for all separations. Deviations are reported with respect to quantum chemistry calculations at the CCSD(T) level from Ref. [70].

Complex	DF1	DF2	DF1-optb88	DF1-cx	DF2-B86R	DF3-opt1	DF3-opt2	VV	SCAN-VV
Hydrogen bonded complexes (7)									
MD [meV]	54.05	31.27	0.84	10.53	9.09	−24.26	−12.01	−18.84	−21.11
MAD [meV]	60.71	34.48	9.40	17.55	11.00	28.42	14.29	20.02	28.75
MARD [%]	14.36	7.01	3.17	6.28	3.02	6.25	3.81	5.11	7.41
WMARD [%]	11.04	5.63	2.17	4.00	2.08	4.72	2.64	3.83	4.71
Complexes with predominant dispersion contribution (8)									
MD [meV]	29.40	30.84	−6.23	2.99	21.57	4.67	3.99	12.75	14.14
MAD [meV]	58.14	36.82	14.59	26.04	21.77	6.25	5.78	15.23	15.12
MARD [%]	135.84	74.36	41.29	67.94	42.88	12.44	13.98	33.09	67.42
WMARD [%]	32.78	17.88	9.92	18.82	13.23	3.67	3.69	7.32	10.11
Mixed complexes (7)									
MD [meV]	17.40	19.25	1.96	5.58	16.00	3.15	3.89	6.60	6.24
MAD [meV]	28.61	19.91	6.67	15.23	16.07	5.91	5.54	7.73	10.34
MARD [%]	26.29	15.10	8.35	17.08	12.24	5.71	6.47	7.12	12.55
WMARD [%]	16.97	11.06	4.30	9.24	8.94	3.62	3.51	4.84	6.56
Average over all separation for all complexes (22)									
MD [meV]	33.43	27.29	−1.37	6.21	15.83	−5.02	−1.13	0.74	0.41
MAD [meV]	49.56	30.70	10.42	19.90	16.53	13.19	8.41	14.37	17.94
MARD [%]	62.33	34.08	18.68	32.14	20.45	8.33	8.35	15.92	30.87
WMARD [%]	20.83	11.81	5.67	11.06	8.32	3.99	3.30	5.42	7.26

TABLE III. Comparison of various statistical measures for the interaction energies of the S66×8 set of molecular dimers for all separations. See caption of Table II for more details. Reference data taken from Ref. [84].

System	DF1	DF2	DF1-optb88	DF1-cx	DF2-B86R	DF3-op1	DF3-opt2	VV	SCAN-VV
Hydrogen bonded complexes (23)									
MD [meV]	32.88	12.81	−3.01	6.47	4.32	−21.20	−14.89	−17.43	−18.08
MAD [meV]	39.45	17.44	7.29	13.87	9.00	22.19	15.27	17.89	20.65
MARD [%]	12.92	4.85	3.36	6.40	3.13	6.46	5.47	5.74	6.27
WMARD [%]	10.00	3.94	2.22	4.12	2.53	5.79	4.60	4.98	5.04
Complexes with predominant dispersion contribution (23)									
MD [meV]	7.65	7.52	−17.68	−2.30	14.19	−4.13	-6.41	−0.57	10.09
MAD [meV]	38.54	20.27	18.02	21.08	15.04	5.91	7.38	8.05	10.87
MARD [%]	69.98	29.83	35.14	42.89	17.45	10.59	12.00	14.74	16.14
WMARD [%]	26.31	13.52	13.35	14.89	9.73	4.73	6.18	5.74	7.85
Others (20)									
MD [meV]	14.69	12.75	−2.65	4.99	13.68	−1.49	−1.68	1.79	1.68
MAD [meV]	28.00	16.14	7.76	15.58	13.93	5.57	5.55	6.31	9.62
MARD [%]	28.62	14.17	10.62	18.80	11.74	4.87	6.24	5.91	9.70
WMARD [%]	17.94	10.12	5.19	10.25	8.88	3.54	3.74	4.12	6.07
Average over all separation for all complexes (66)									
MD [meV]	18.57	10.95	−8.02	2.97	10.59	−9.28	−7.93	−5.73	−2.28
MAD [meV]	35.66	18.03	11.17	16.90	12.60	11.48	9.58	10.95	13.90
MARD [%]	37.56	16.38	16.64	22.87	10.73	7.42	7.98	8.93	10.75
WMARD [%]	18.09	9.15	7.00	9.73	6.96	4.74	4.89	4.98	6.33

TABLE IV. Lattice constants [Å] and atomization energies [eV] for selected solids. Zero-point corrected experimental lattice constants and atomization energies are taken from Ref. [39, 75, 86] and references therein; SCAN-VV data taken from Ref. [75].

System	expt.	PBE	PBEsol	DF1	DF2	DF1-optB88	DF1-cx	DF2-B86R	DF3-opt1	DF3-opt2	VV	SCAN-VV
Lattice constants												
Cu	3.60	3.63	3.56	3.69	3.75	3.62	3.57	3.59	3.57	3.59	3.65	3.54
Ag	4.06	4.15	4.05	4.25	4.33	4.14	4.07	4.11	4.08	4.10	4.17	4.06
Pd	3.88	3.95	3.88	4.01	4.09	3.94	3.89	3.92	3.90	3.91	3.98	3.88
Rh	3.79	3.83	3.78	3.88	3.95	3.84	3.79	3.81	3.80	3.81	3.87	3.77
Na	4.21	4.20	4.17	4.21	4.14	4.15	4.24	4.17	4.14	4.15	4.13	4.15
K	5.21	5.28	5.21	5.31	5.20	5.21	5.32	5.24	5.22	5.21	5.14	5.23
Rb	5.58	5.67	5.57	5.60	5.51	5.49	5.59	5.53	5.48	5.51	5.46	5.59
Cs	6.04	6.16	6.01	6.00	5.93	5.83	5.90	5.89	5.80	5.86	5.84	6.05
Ca	5.55	5.53	5.46	5.54	5.48	5.44	5.46	5.46	5.41	5.44	5.46	5.52
Sr	6.05	6.03	5.92	6.07	6.02	5.92	5.93	5.94	5.88	5.92	5.93	6.04
Ba	5.00	5.02	4.88	5.07	5.05	4.91	4.87	4.92	4.85	4.90	4.92	4.98
Al	4.02	4.04	4.01	4.09	4.09	4.06	4.03	4.04	4.03	4.04	4.03	4.00
LiF	3.96	4.07	4.01	4.11	4.08	4.03	4.06	4.04	4.00	4.02	4.03	3.94
LiCl	5.06	5.15	5.06	5.22	5.21	5.12	5.11	5.11	5.06	5.09	5.11	5.04
NaF	4.58	4.72	4.65	4.76	4.70	4.66	4.71	4.67	4.62	4.65	4.65	4.53
NaCl	5.57	5.70	5.61	5.75	5.70	5.63	5.67	5.64	5.58	5.61	5.61	5.51
MgO	4.18	4.26	4.22	4.28	4.29	4.23	4.23	4.23	4.21	4.23	4.25	4.17
C	3.54	3.57	3.56	3.59	3.61	3.58	3.57	3.57	3.57	3.57	3.59	3.55
SiC	4.34	4.38	4.36	4.40	4.43	4.38	4.37	4.38	4.37	4.37	4.40	4.35
Si	5.42	5.47	5.44	5.51	5.55	5.48	5.44	5.46	5.45	5.46	5.50	5.42
Ge	5.64	5.76	5.67	5.84	5.94	5.73	5.67	5.71	5.68	5.70	5.80	5.63
GaAs	5.64	5.75	5.67	5.84	5.93	5.74	5.68	5.72	5.69	5.71	5.79	5.64
MD [Å]	—	0.06	0.00	0.10	0.09	0.01	0.01	0.01	−0.02	−0.002	0.02	−0.01
MAD [Å]	—	0.07	0.04	0.10	0.13	0.07	0.06	0.06	0.06	0.06	0.09	0.02
MARD [%]	—	1.44	0.73	2.20	2.75	1.47	1.14	1.17	1.10	1.12	1.80	0.43
Atomization energies												
Cu	3.52	3.53	4.10	3.07	2.89	3.59	3.90	3.70	3.95	3.79	3.72	4.04
Ag	2.98	2.52	3.09	2.29	2.15	2.76	2.98	2.79	3.07	2.88	2.89	3.08
Pd	3.94	3.74	4.46	3.36	3.16	4.00	4.32	4.09	4.39	4.19	4.13	4.59
Rh	5.78	5.74	6.68	4.99	4.69	6.06	6.72	6.26	6.73	6.44	5.92	5.60
Na	1.12	1.05	1.12	0.96	0.96	0.99	1.20	1.01	1.06	1.04	1.07	1.14
K	0.94	0.86	0.92	0.82	0.73	0.85	0.90	0.84	0.89	0.86	0.94	0.91
Rb	0.86	0.77	0.83	0.77	0.66	0.78	0.81	0.76	0.82	0.79	0.87	0.82
Cs	0.81	0.71	0.78	0.79	0.64	0.76	0.77	0.72	0.79	0.75	0.87	0.75
Ca	1.86	1.91	2.10	1.66	1.40	1.86	2.04	1.87	2.02	1.91	2.00	2.17
Sr	1.73	1.61	1.81	1.42	1.12	1.61	1.78	1.60	1.76	1.63	1.73	1.91
Ba	1.91	1.88	2.13	1.79	1.49	1.99	2.14	1.95	2.13	1.99	2.10	2.15
Al	3.43	3.47	3.81	2.90	2.52	3.24	3.64	3.43	3.58	3.49	3.41	3.71
LiF	4.46	4.39	4.49	4.44	4.57	4.56	4.44	4.49	4.59	4.55	4.55	4.49
LiCl	3.59	3.36	3.49	3.42	3.44	3.54	3.51	3.49	3.59	3.54	3.53	3.58
NaF	3.97	3.89	3.96	3.97	4.08	4.04	4.02	3.97	3.98	4.01	4.03	4.00
NaCl	3.34	3.09	3.20	3.18	3.19	3.26	3.29	3.19	3.29	3.23	3.24	3.33
MgO	5.20	5.11	5.38	4.95	4.93	5.06	5.27	5.20	5.26	5.26	5.26	5.34
C	7.55	7.70	8.18	7.13	6.87	7.60	7.89	7.76	7.97	7.85	7.61	7.60
SiC	6.48	6.38	6.79	5.95	5.72	6.38	6.61	6.48	6.68	6.56	6.34	6.55
Si	4.68	4.51	4.86	4.19	4.00	4.55	4.75	4.62	4.80	4.69	4.57	4.82
Ge	3.92	3.69	4.08	3.30	3.31	3.82	3.98	3.84	4.05	3.91	3.86	4.10
GaAs	3.34	3.13	3.54	2.85	2.80	3.27	3.40	3.27	3.50	3.34	3.35	3.47
MD [eV]	—	−0.11	0.20	−0.33	−0.46	−0.04	0.13	−0.004	0.16	0.06	0.03	0.12
MAD [eV]	—	0.13	0.23	0.33	0.48	0.10	0.16	0.10	0.18	0.12	0.08	0.15
MARD [%]	—	5.03	6.24	10.19	16.31	4.08	4.87	4.24	5.08	3.99	2.90	5.47

TABLE V. Layer separation [Å] and layer binding energies [meV/Å^2] for selected layered structures. Reference data for the separation is taken from experiment and for the binding energy from RPA, as detailed in Ref. [77, 78] and references therein. SCAN-VV data taken from Ref. [75].

System	ref.	DF1	DF2	DF1-optB88	DF1-cx	DF2-B86R	DF3-opt1	DF3-opt2	VV	SCAN-VV
Layer separation										
BN	3.35	3.54	3.47	3.28	3.21	3.26	3.24	3.23	3.29	3.24
graphite	3.35	3.55	3.49	3.34	3.28	3.31	3.31	3.29	3.35	3.27
HfS_2	5.84	5.95	6.00	5.82	5.75	5.78	5.74	5.77	5.87	5.79
$HfSe_2$	6.16	6.46	6.53	6.30	6.23	6.27	6.22	6.26	6.39	6.14
$HfTe_2$	6.65	7.25	7.27	6.78	6.55	6.67	6.59	6.63	6.81	6.69
MoS_2	6.15	6.62	6.57	6.26	6.12	6.18	6.14	6.15	6.24	6.14
$MoSe_2$	6.46	7.03	7.02	6.62	6.45	6.54	6.48	6.51	6.62	6.51
$PdTe_2$	5.11	5.65	6.02	5.36	5.14	5.25	5.19	5.23	5.48	5.00
WS_2	6.16	6.58	6.53	6.28	6.15	6.21	6.17	6.18	6.26	6.12
MD [Å]	—	0.58	0.59	0.12	−0.07	0.03	−0.03	−0.01	0.15	−0.04
MAD [Å]	—	0.58	0.59	0.16	0.09	0.10	0.08	0.09	0.18	0.06
MARD [%]	—	6.81	7.26	1.96	1.30	1.31	1.13	1.29	2.35	1.22
Layer binding energy										
BN	14.4	19.02	18.30	25.33	23.80	21.17	20.17	22.04	24.73	18.45
graphite	18.3	20.54	20.21	27.00	25.27	23.28	21.01	23.95	26.81	20.30
HfS_2	16.1	15.08	16.33	21.51	20.20	19.16	17.90	20.25	23.42	15.85
$HfSe_2$	17.0	15.68	16.22	21.38	20.48	19.08	18.08	19.94	23.76	16.10
$HfTe_2$	18.6	15.72	16.04	22.71	24.55	21.97	21.37	23.04	26.93	17.99
MoS_2	20.5	18.76	19.61	25.73	24.36	23.28	21.41	24.14	29.74	19.89
$MoSe_2$	19.6	17.52	18.10	24.73	24.37	22.34	21.11	23.04	29.61	19.33
$PdTe_2$	40.1	23.59	21.73	42.86	51.60	44.33	46.73	45.95	47.43	41.74
WS_2	20.2	18.07	18.84	25.83	24.23	23.17	21.42	23.97	29.97	23.38
MD [meV/Å^2]	—	−2.31	−2.16	5.81	5.43	3.67	2.71	4.61	8.62	0.91
MAD [meV/Å^2]	—	3.84	3.50	5.81	5.43	3.67	2.71	4.61	8.62	1.50
MARD [%]	—	16.08	13.53	32.36	26.31	19.60	13.55	24.38	45.67	8.15

TABLE VI. Lattice constants a, b, and c [Å], unit cell angles α, β, and γ [°], volume per monomer [Å^3], and cohesive energy per monomer [eV] for molecular crystals formed from benzene, naphthalene, anthracene, and tetracene. Relative deviation (RD) are given for the volume and energy. Experimental reference data taken from Ref. [12] and references therein. Reference data for the cohesive energy is not available for tetracene.

System	expt.	DF1	DF2	DF1-optB88	DF1-cx	DF2-B86R	DF2-opt1	DF2-opt2	VV
Benzene	$T = 4$K								
a [Å]	7.36	7.607	7.458	7.443	7.450	7.353	7.247	7.288	7.294
b [Å]	9.37	9.644	9.398	9.443	9.581	9.336	9.193	9.240	9.209
c [Å]	6.70	7.082	6.899	6.855	6.809	6.713	6.573	6.623	6.642
vol./monomer [Å^3]	115.5	129.9	120.9	120.5	121.5	115.2	109.5	111.5	111.6
RD [%]	—	12.5	4.71	4.33	5.24	−0.20	−5.17	−3.42	−3.38
coh. energy/monomer [eV]	0.520	0.624	0.585	0.755	0.628	0.559	0.649	0.637	0.659
RD [%]	—	20.0	12.5	45.1	20.8	7.49	24.74	22.50	26.7
Naphthalene	$T = 5$K								
a [Å]	8.08	8.405	8.215	7.995	8.117	8.032	7.917	7.948	7.981
b [Å]	5.93	6.069	5.985	5.884	5.939	5.906	5.853	5.872	5.877
c [Å]	8.63	8.714	8.592	8.578	8.795	8.623	8.555	8.578	8.520
β [°]	124.7	121.7	122.5	123.8	124.1	124.1	124.7	124.4	124.1
vol./monomer [Å^3]	170.2	189.2	178.2	167.6	175.7	169.4	163.0	165.1	165.6
RD [%]	—	11.16	4.72	−1.52	3.20	−0.47	−4.22	−2.98	−2.72
coh. energy/monomer [eV]	0.820	0.979	0.931	0.892	0.994	0.892	0.995	0.994	1.054
RD [%]	—	19.42	13.54	8.77	21.25	8.79	21.39	21.15	28.48
Anthracene	$T = 16$K								
a [Å]	8.37	8.732	8.560	8.321	8.431	8.355	8.250	8.275	8.307
b [Å]	6.00	6.116	6.027	5.937	5.988	5.957	5.906	5.924	5.923
c [Å]	11.12	11.24	11.10	11.04	11.29	11.09	11.01	11.04	10.98
β [°]	125.4	123.6	124.2	125.1	125.5	125.3	125.7	125.6	125.2
vol./monomer [Å^3]	227.6	245.0	236.9	223.1	232.0	225.2	217.8	220.1	220.8
RD [%]	—	9.84	4.08	−1.96	1.92	−1.06	−4.33	−3.32	−2.98
coh. energy/monomer [eV]	1.130	1.360	1.304	1.255	1.392	1.257	1.374	1.380	1.478
RD [%]	—	20.32	15.36	11.03	23.15	11.22	21.57	22.12	30.79
Tetracene	$T = 0$K								
a [Å]	6.03	6.163	6.083	6.000	6.083	6.028	5.981	5.996	5.983
b [Å]	7.71	8.185	7.967	7.695	7.739	7.710	7.600	7.624	7.670
c [Å]	12.88	13.365	13.167	12.917	12.978	12.914	12.773	12.832	12.878
α [°]	77.60	75.47	76.05	77.41	77.90	77.54	77.99	77.87	77.39
β [°]	72.10	71.45	71.66	72.10	72.69	72.25	72.36	72.28	72.07
γ [°]	85.50	86.27	86.02	85.72	85.45	85.56	85.46	85.53	85.67
vol./monomer [Å^3]	278.9	309.3	293.9	276.9	285.1	279.1	270.6	273.1	274.3
RD [%]	—	10.92	5.39	−0.70	2.23	0.08	−2.98	−2.05	−1.63
coh. energy/monomer [eV]	—	1.748	1.694	1.628	1.800	1.640	1.775	1.789	1.930

TABLE VII. Adsorption distance [Å] defined as the carbon–metal distance, adsorption energy [eV], and their relative deviation (RD) for benzene adsorbed on the (111) surface of Cu, Ag, and Au. Reference data is available in Refs. [75, 79–82]. For SCAN-VV we report the distance between the surface and the center of mass of the benzene molecule [75].

System	expt.	DF1	DF2	DF1-optB88	DF1-cx	DF2-B86R	DF3-opt1	DF3-opt2	VV	SCAN-VV
Cu(111)/benzene										
distance [Å]	2.83	3.60	3.49	3.34	2.95	3.10	2.87	3.01	3.13	2.93
RD [%]	—	27.92	24.05	18.62	4.51	10.13	1.86	7.04	11.31	3.53
energy [eV]	0.68±0.04	0.464	0.430	0.595	0.708	0.530	0.646	0.617	0.697	0.740
RD [%]	—	−31.74	−36.82	−12.52	4.06	−22.04	−4.95	−9.20	2.50	8.82
Ag(111)/benzene										
distance [Å]	2.97	3.58	3.45	3.33	3.05	3.14	2.99	3.07	3.14	3.02
RD [%]	—	20.44	16.05	12.24	2.64	5.61	0.54	3.28	5.85	1.68
energy [eV]	0.63±0.05	0.513	0.478	0.673	0.669	0.608	0.655	0.668	0.767	0.680
RD [%]	—	−18.63	−24.10	6.82	6.20	−3.47	4.02	5.99	21.71	7.94
Au(111)/benzene										
distance [Å]	3.05	3.50	3.36	3.28	3.06	3.12	3.01	3.06	3.11	3.07
RD [%]	—	14.81	10.15	7.55	0.20	2.18	1.47	0.28	2.10	0.66
energy [eV]	0.71±0.03	0.601	0.575	0.771	0.767	0.653	0.724	0.712	0.839	0.730
RD [%]	—	−15.39	−18.97	8.57	7.97	−8.00	1.96	0.21	18.11	2.82

[1] K. Tan, S. Zuluaga, E. Fuentes, E. C. Mattson, J.-F. Veyan, H. Wang, J. Li, T. Thonhauser, and Y. J. Chabal, Trapping gases in metal-organic frameworks with a selective surface molecular barrier layer, Nat. Commun. **7**, 13871 (2016).

[2] H. Wang, X. Dong, J. Lin, S. J. Teat, S. Jensen, J. Cure, E. V. Alexandrov, Q. Xia, K. Tan, Q. Wang, D. H. Olson, D. M. Proserpio, Y. J. Chabal, T. Thonhauser, J. Sun, Y. Han, and J. Li, Topologically guided tuning of Zr-MOF pore structures for highly selective separation of C_6 alkane isomers, Nat. Commun. **9**, 1745 (2018).

[3] B. Li, X. Dong, H. Wang, D. Ma, K. Tan, S. Jensen, B. J. Deibert, J. Butler, J. Cure, Z. Shi, T. Thonhauser, Y. J. Chabal, Y. Han, and J. Li, Capture of organic iodides from nuclear waste by metal-organic framework-based molecular traps, Nat. Commun. **8**, 485 (2017).

[4] S. Jensen, K. Tan, W. P. Lustig, D. S. Kilin, J. Li, Y. J. Chabal, and T. Thonhauser, Structure-driven photoluminescence enhancement in a Zn-based metal-organic framework, Chem. Mater. **31**, 7933 (2019).

[5] J. Cure, E. Mattson, K. Cocq, H. Assi, S. Jensen, K. Tan, M. Catalano, S. Yuan, H. Wang, L. Feng, P. Zhang, S. Kwon, J.-F. Veyan, Y. Cabrera, G. Zhang, J. Li, M. Kim, H.-C. Zhou, Y. J. Chabal, and T. Thonhauser, High stability of ultra-small and isolated gold nanoparticles in metal-organic framework materials, J. Mater. Chem. A **7**, 17536 (2019).

[6] P. J. Diemer, J. Hayes, E. Welchman, R. Hallani, S. J. Pookpanratana, C. A. Hacker, C. A. Richter, J. E. Anthony, T. Thonhauser, and O. D. Jurchescu, The influence of isomer purity on trap states and performance of organic thin-film transistors, Adv. Electron. Mater. **3**, 1600294 (2017).

[7] R. Gomez-Bombarelli, J. Aguilera-Iparraguirre, T. D. Hirzel, D. Duvenaud, D. Maclaurin, M. A. Blood-Forsythe, H. S. Chae, M. Einzinger, D.-G. Ha, T. Wu, G. Markopoulos, S. Jeon, H. Kang, H. Miyazaki, M. Numata, S. Kim, W. Huang, S. I. Hong, M. Baldo, R. P. Adams, and A. Aspuru-Guzik, Design of efficient molecular organic light-emitting diodes by a high-throughput virtual screening and experimental approach, Nat. Mater. **15**, 1120 (2016).

[8] A. M. Reilly and A. Tkatchenko, Role of dispersion interactions in the polymorphism and entropic stabilization of the aspirin crystal, Phys. Rev. Lett. **113**, 055701 (2014).

[9] K. Lee, B. Kolb, T. Thonhauser, D. Vanderbilt, and D. C. Langreth, Structure and energetics of a ferroelectric organic crystal of phenazine and chloranilic acid, Phys. Rev. B **86**, 104102 (2012).

[10] S. Ishibashi, S. Horiuchi, and R. Kumai, Computational findings of metastable ferroelectric phases of squaric acid, Phys. Rev. B **97**, 184102 (2018).

[11] L. Kronik and A. Tkatchenko, Understanding molecular crystals with dispersion-inclusive density functional theory: Pairwise corrections and beyond, Acc. Chem. Res. **47**, 3208 (2014).

[12] T. Rangel, K. Berland, S. Sharifzadeh, F. Brown-Altvater, K. Lee, P. Hyldgaard, L. Kronik, and J. B. Neaton, Structural and excited-state properties of oligoacene crystals from first principles, Phys. Rev. B **93**, 115206 (2016).

[13] S. Grimme, Accurate description of van der Waals complexes by density functional theory including empirical corrections, J. Comput. Chem. **25**, 1463 (2004).

[14] S. Grimme, J. Antony, T. Schwabe, and C. Mück-Lichtenfeld, Density functional theory with dispersion corrections for supramolecular structures, aggregates, and complexes of (bio)organic molecules, Org. Biomol. Chem. **5**, 741 (2007).

[15] S. Grimme, Density functional theory with London dispersion corrections, WIREs Comput. Mol. Sci. **1**, 211 (2011).

[16] A. Tkatchenko and M. Scheffler, Accurate molecular van der Waals interactions from ground-state electron density and free-atom reference data, Phys. Rev. Lett. **102**, 073005 (2009).

[17] A. Tkatchenko, R. A. DiStasio, R. Car, and M. Scheffler, Accurate and efficient method for many-body van der Waals interactions, Phys. Rev. Lett. **108**, 236402 (2012).

[18] A. Ambrosetti, A. M. Reilly, R. A. DiStasio, and A. Tkatchenko, Long-range correlation energy calculated from coupled atomic response functions, J. Chem. Phys. **140**, 18A508 (2014).

[19] A. Ambrosetti, N. Ferri, R. A. DiStasio, and A. Tkatchenko, Wavelike charge density fluctuations and van der Waals interactions at the nanoscale, Science **351**, 1171 (2016).

[20] O. A. Vydrov and T. Van Voorhis, Nonlocal van der Waals density functional made simple, Phys. Rev. Lett. **103**, 063004 (2009).

[21] O. A. Vydrov and T. Van Voorhis, Dispersion interactions from a local polarizability model, Phys. Rev. A **81**, 062708 (2010).

[22] O. A. Vydrov and T. Van Voorhis, Nonlocal van der Waals density functional: The simpler the better, J. Chem. Phys. **133**, 244103 (2010).

[23] S. Grimme, A. Hansen, J. G. Brandenburg, and C. Bannwarth, Dispersion-corrected mean-field electronic structure methods, Chem. Rev. **116**, 5105 (2016).

[24] K. Szalewicz, Symmetry-adapted perturbation theory of intermolecular forces, WIREs Comput. Mol. Sci. **2**, 254 (2012).

[25] L. A. Burns, A. Vazquez-Mayagoitia, B. G. Sumpter, and C. D. Sherrill, Density-functional approaches to noncovalent interactions: A comparison of dispersion corrections (DFT-D), exchange-hole dipole moment (XDM) theory, and specialized functionals, J. Chem. Phys. **134**, 084107 (2011).

[26] J. Klimes and A. Michaelides, Perspective: Advances and challenges in treating van der Waals dispersion forces in density functional theory, J. Chem. Phys. **137**, 120901 (2012).

[27] M. Dion, H. Rydberg, E. Schröder, D. C. Langreth, and B. I. Lundqvist, van der Waals density functional for general geometries, Phys. Rev. Lett. **92**, 246401 (2004).

[28] T. Thonhauser, S. Zuluaga, C. A. Arter, K. Berland, E. Schröder, and P. Hyldgaard, Spin signature of nonlocal correlation binding in metal-organic frameworks, Phys. Rev. Lett. **115**, 136402 (2015).

[29] D. C. Langreth, B. I. Lundqvist, S. D. Chakarova-Käck, V. R. Cooper, M. Dion, P. Hyldgaard, A. Kelkkanen, J. Kleis, L. Kong, S. Li, P. G. Moses, E. D. Murray,

A. Puzder, H. Rydberg, E. Schröder, and T. Thonhauser, A density functional for sparse matter, J. Phys.: Condens. Matter **21**, 084203 (2009).

[30] K. Berland, V. R. Cooper, K. Lee, E. Schröder, T. Thonhauser, P. Hyldgaard, and B. I. Lundqvist, van der Waals forces in density functional theory: A review of the vdW-DF method, Rep. Prog. Phys. **78**, 066501 (2015).

[31] P. Hyldgaard, Y. Jiao, and V. Shukla, Screening nature of the van der Waals density functional method: A review and analysis of the many-body physics foundation, J. Phys.: Condens. Mat. (2020).

[32] K. Berland, C. A. Arter, V. R. Cooper, K. Lee, B. I. Lundqvist, E. Schröder, T. Thonhauser, and P. Hyldgaard, van der Waals density functionals built upon the electron-gas tradition: Facing the challenge of competing interactions, J. Chem. Phys. **140**, 18A539 (2014).

[33] K. Lee, K. Kelkkanen, K. Berland, S. Andersson, D. Langreth, E. Schröder, B. Lundqvist, and P. Hyldgaard, Evaluation of a density functional with account of van der Waals forces using experimental data of H_2 physisorption on Cu (111), Phys. Rev. B **84**, 193408 (2011).

[34] W. Hujo and S. Grimme, Comparison of the performance of dispersion-corrected density functional theory for weak hydrogen bonds, Phys. Chem. Chem. Phys. **13**, 13942 (2011).

[35] T. Gould, E. R. Johnson, and S. A. Tawfik, Are dispersion corrections accurate outside equilibrium? A case study on benzene, Beilstein J. Org. Chem. **14**, 1181 (2018).

[36] V. R. Cooper, van der Waals density functional: An appropriate exchange functional, Phys. Rev. B **81**, 161104 (2010).

[37] J. Klimeš, D. R. Bowler, and A. Michaelides, Chemical accuracy for the van der Waals density functional, J. Phys. Condens. Matter **22**, 022201 (2010).

[38] J. Wellendorff, K. T. Lundgaard, A. Møgelhøj, V. Petzold, D. D. Landis, J. K. Nørskov, T. Bligaard, and K. W. Jacobsen, Density functionals for surface science: Exchange-correlation model development with Bayesian error estimation, Phys. Rev. B **85**, 235149 (2012).

[39] J. Klimeš, D. R. Bowler, and A. Michaelides, van der Waals density functionals applied to solids, Phys. Rev. B **83**, 195131 (2011).

[40] K. Berland and P. Hyldgaard, Exchange functional that tests the robustness of the plasmon description of the van der Waals density functional, Phys. Rev. B **89**, 035412 (2014).

[41] I. Hamada, van der Waals density functional made accurate, Phys. Rev. B **89**, 121103 (2014).

[42] E. D. Murray, K. Lee, and D. C. Langreth, Investigation of exchange energy density functional accuracy for interacting molecules, J. Chem. Theory Comput. **5**, 2754 (2009).

[43] K. Lee, E. D. Murray, L. Kong, B. I. Lundqvist, and D. C. Langreth, Higher-accuracy van der Waals density functional, Phys. Rev. B **82**, 081101 (2010).

[44] T. Thonhauser, V. R. Cooper, S. Li, A. Puzder, P. Hyldgaard, and D. C. Langreth, van der Waals density functional: Self-consistent potential and the nature of the van der Waals bond, Phys. Rev. B **76**, 125112 (2007).

[45] H. Rydberg, M. Dion, N. Jacobson, E. Schröder, P. Hyldgaard, S. I. Simak, D. C. Langreth, and B. I. Lundqvist, van der Waals density functional for layered structures, Phys. Rev. Lett. **91**, 126402 (2003).

[46] O. A. Vydrov and T. Van Voorhis, Improving the accuracy of the nonlocal van der Waals density functional with minimal empiricism, J. Chem. Phys. **130**, 104105 (2009).

[47] H. Rydberg, *Nonlocal Correlations in Density Functional Theory*, Ph.D. thesis, Chalmers University of Technology and Göteborg University (2001).

[48] K. Berland, *Connected by Voids: Interactions and Screening in Sparse Matter*, Ph.D. thesis, Chalmers University of Technology (2012).

[49] P. Hyldgaard, K. Berland, and E. Schröder, Interpretation of van der Waals density functionals, Phys. Rev. B **90**, 075148 (2014).

[50] E. Schröder, V. R. Cooper, K. Berland, B. I. Lundqvist, P. Hyldgaard, and T. Thonhauser, The vdW-DF family of nonlocal exchange-correlation functionals, in *Non-Covalent Interact. Quantum Chem. Phys. Theory Appl.*, edited by A. O. de la Roza and G. A. DiLabio (Elsevier, Amsterdam, 2017) Chap. 8, pp. 241–274.

[51] K. Berland, D. Chakraborty, and T. Thonhauser, van der Waals density functional with corrected C_6 coefficients, Phys. Rev. B **99**, 195418 (2019).

[52] J. P. Perdew, K. Burke, and Y. Wang, Generalized gradient approximation for the exchange-correlation hole of a many-electron system, Phys. Rev. B **54**, 16533 (1996).

[53] Y. Zhang and W. Yang, Comment on "Generalized gradient approximation made simple", Phys. Rev. Lett. **80**, 890 (1998).

[54] I. Hamada and M. Otani, Comparative van der Waals density-functional study of graphene on metal surfaces, Phys. Rev. B **82**, 153412 (2010).

[55] H. Yildirim, T. Greber, and A. Kara, Trends in adsorption characteristics of benzene on transition metal surfaces: Role of surface chemistry and van der Waals interactions, J. Phys. Chem. C **117**, 20572 (2013).

[56] W. Liu, J. Carrasco, B. Santra, A. Michaelides, M. Scheffler, and A. Tkatchenko, Benzene adsorbed on metals: Concerted effect of covalency and van der Waals bonding, Phys. Rev. B **86**, 245405 (2012).

[57] S. D. Chakarova-Kack, E. Schröder, B. I. Lundqvist, and D. C. Langreth, Application of van der Waals density functional to an extended system: Adsorption of benzene and naphthalene on graphite, Phys. Rev. Lett. **96**, 146107 (2006).

[58] V. R. Cooper, T. Thonhauser, A. Puzder, E. Schröder, B. I. Lundqvist, and D. C. Langreth, Stacking interactions and the twist of DNA, J. Am. Chem. Soc. **130**, 1304 (2008).

[59] J. Kleis, E. Schröder, and P. Hyldgaard, Nature and strength of bonding in a crystal of semiconducting nanotubes: van der Waals density functional calculations and analytical results, Phys. Rev. B. **77**, 205422 (2008).

[60] G. Román-Pérez and J. M. Soler, Efficient implementation of a van der Waals density functional: Application to double-wall carbon nanotubes, Phys. Rev. Lett. **103**, 096102 (2009).

[61] K. Toyoda, Y. Nakano, I. Hamada, K. Lee, S. Yanagisawa, and Y. Morikawa, First-principles study of benzene on noble metal surfaces: Adsorption states and vacuum level shifts, Surf. Sci. **603**, 2912 (2009).

[62] J. P. Perdew and Y. Wang, Accurate and simple density functional for the electronic exchange energy: Generalized gradient approximation, Phys. Rev. B **33**, 8800

(1986).
[63] K. Berland and P. Hyldgaard, Analysis of van der Waals density functional components: Binding and corrugation of benzene and C_{60} on boron nitride and graphene, Phys. Rev. B **87**, 205421 (2013).
[64] T. Bjorkman, A. Gulans, A. V. Krasheninnikov, and R. M. Nieminen, Are we van der Waals ready?, J. Phys.: Condens. Mat. **24**, 424218 (2012).
[65] F. Tran, L. Kalantari, B. Traore, X. Rocquefelte, and P. Blaha, Nonlocal van der Waals functionals for solids: Choosing an appropriate one, Phys. Rev. Mater. **3**, 063602 (2019).
[66] J. P. Perdew, A. Ruzsinszky, G. I. Csonka, O. A. Vydrov, G. E. Scuseria, L. A. Constantin, X. Zhou, and K. Burke, Restoring the density-gradient expansion for exchange in solids and surfaces, Phys. Rev. Lett. **100**, 136406 (2008).
[67] This functional is occasionally called rev-vdW-DF2, but we do not employ this nomenclature, as it was only the exchange that was revised.
[68] F. Tran and J. Hutter, Nonlocal van der Waals functionals: The case of rare-gas dimers and solids, J. Chem. Phys. **138**, 204103 (2013).
[69] A. H. Larsen, M. Kuisma, J. Lfgren, Y. Pouillon, P. Erhart, and P. Hyldgaard, libvdwxc: A library for exchangecorrelation functionals in the vdW-DF family, Model. Simul. Mater. Sci. Eng. **25**, 065004 (2017).
[70] L. Gráfová, M. Pitoňák, J. Řezáč, and P. Hobza, Comparative study of selected wave function and density functional methods for noncovalent interaction energy calculations using the extended S22 data set, J. Chem. Theory Comput. **6**, 2365 (2010).
[71] The exchange part depends on β and γ only through the changes in density in fully self-consistent calculations. The same is true for the dependence of the non-local correlation on κ.
[72] P. Giannozzi, O. Andreussi, T. Brumme, O. Bunau, M. Buongiorno Nardelli, M. Calandra, R. Car, C. Cavazzoni, D. Ceresoli, M. Cococcioni, N. Colonna, I. Carnimeo, A. Dal Corso, S. de Gironcoli, P. Delugas, R. A. DiStasio, A. Ferretti, A. Floris, G. Fratesi, G. Fugallo, R. Gebauer, U. Gerstmann, F. Giustino, T. Gorni, J. Jia, M. Kawamura, H.-Y. Ko, A. Kokalj, E. Küçükbenli, M. Lazzeri, M. Marsili, N. Marzari, F. Mauri, N. L. Nguyen, H.-V. Nguyen, A. Otero-de-la Roza, L. Paulatto, S. Poncé, D. Rocca, R. Sabatini, B. Santra, M. Schlipf, A. P. Seitsonen, A. Smogunov, I. Timrov, T. Thonhauser, P. Umari, N. Vast, X. Wu, and S. Baroni, Advanced capabilities for materials modelling with Quantum ESPRESSO, J. Phys.: Condens. Matter **29**, 465901 (2017).
[73] K. F. Garrity, J. W. Bennett, K. M. Rabe, and D. Vanderbilt, Pseudopotentials for high-throughput DFT calculations, Comput. Mater. Sci. **81**, 446 (2014).
[74] R. Sabatini, T. Gorni, and S. de Gironcoli, Nonlocal van der Waals density functional made simple and efficient, Phys. Rev. B **87**, 041108(R) (2013).
[75] H. Peng, Z.-H. Yang, J. P. Perdew, and J. Sun, Versatile van der Waals density functional based on a meta-generalized gradient approximation, Phys. Rev. X **6**, 041005 (2016).
[76] J. P. Perdew, K. Burke, and M. Ernzerhof, Generalized gradient approximation made simple, Phys. Rev. Lett. **77**, 3865 (1996).
[77] T. Björkman, A. Gulans, A. V. Krasheninnikov, and R. M. Nieminen, van der Waals bonding in layered compounds from advanced density-functional first-principles calculations, Phys. Rev. Lett. **108**, 235502 (2012).
[78] T. Björkman, Testing several recent van der Waals density functionals for layered structures, J. Chem. Phys. **141**, 074708 (2014).
[79] K. Berland, T. L. Einstein, and P. Hyldgaard, Rings sliding on a honeycomb network: Adsorption contours, interactions, and assembly of benzene on Cu (111), Phys. Rev. B **80**, 155431 (2009).
[80] W. Liu, V. G. Ruiz, G.-X. Zhang, B. Santra, X. Ren, M. Scheffler, and A. Tkatchenko, Structure and energetics of benzene adsorbed on transition-metal surfaces: Density-functional theory with van der Waals interactions including collective substrate response, New J. Phys. **15**, 053046 (2013).
[81] A. Bilic, J. R. Reimers, N. S. Hush, R. C. Hoft, and M. J. Ford, Adsorption of benzene on copper, silver, and gold surfaces, J. Chem. Theory Comput. **2**, 1093 (2006).
[82] F. Maaß, Y. Jiang, W. Liu, A. Tkatchenko, and P. Tegeder, Binding energies of benzene on coinage metal surfaces: Equal stability on different metals, J. Chem. Phys. **148**, 214703 (2018).
[83] See Supplemental Material at XXX for additional and more detailed computational results of the S22, S22×5, S66, and S66×8 datasets.
[84] J. Řezáč, K. E. Riley, and P. Hobza, S66: A well-balanced database of benchmark interaction energies relevant to biomolecular structures, J. Chem. Theory Comput. **7**, 2427 (2011).
[85] D. W. Scott, On optimal and data-based histograms, Biometrika **66**, 605 (1979).
[86] G. I. Csonka, J. P. Perdew, A. Ruzsinszky, P. H. T. Philipsen, S. Lebègue, J. Paier, O. A. Vydrov, and J. G. Ángyán, Assessing the performance of recent density functionals for bulk solids, Phys. Rev. B **79**, 155107 (2009).
[87] We chose this set as the intersection of the sets given in Refs. [37, 39, 75].
[88] K. Berland, Ø. Borck, and P. Hyldgaard, van der Waals density functional calculations of binding in molecular crystals, Comp. Phys. Commun. **182**, 1800 (2011).
[89] D. J. Carter and A. L. Rohl, Benchmarking calculated lattice parameters and energies of molecular crystals using van der Waals density functionals, J. Chem. Theory Comp. **10**, 3423 (2014).
[90] A. Otero-de-la Roza and E. R. Johnson, A benchmark for non-covalent interactions in solids, J. Chem. Phys. **137**, 054103 (2012).
[91] Q. Peng, G. Wang, G.-R. Liu, and S. De, van der Waals density functional theory vdW-DFq for semihard materials, Cryst. **9**, 243 (2019).
[92] A. M. Reilly and A. Tkatchenko, Understanding the role of vibrations, exact exchange, and many-body van der Waals interactions in the cohesive properties of molecular crystals, J. Chem. Phys. **139**, 024705 (2013).
[93] K. Lee, K. Berland, M. Yoon, S. Andersson, E. Schrder, P. Hyldgaard, and B. I. Lundqvist, Benchmarking van der Waals density functionals with experimental data: Potential-energy curves for H_2 molecules on Cu (111), (100) and (110) surfaces, J. Phys.: Condens. Matter **24**, 424213 (2012).